



# The role of mixing in the large-scale ocean circulation

Casimir de Lavergne, Sjoerd Groeskamp, Jan Zika, Helen L Johnson

## ► To cite this version:

Casimir de Lavergne, Sjoerd Groeskamp, Jan Zika, Helen L Johnson. The role of mixing in the large-scale ocean circulation. Ocean Mixing, Elsevier, pp.35-63, 2022, 10.1016/B978-0-12-821512-8.00010-4 . hal-03372726

**HAL Id: hal-03372726**

**<https://hal.science/hal-03372726>**

Submitted on 11 Oct 2021

**HAL** is a multi-disciplinary open access archive for the deposit and dissemination of scientific research documents, whether they are published or not. The documents may come from teaching and research institutions in France or abroad, or from public or private research centers.

L'archive ouverte pluridisciplinaire **HAL**, est destinée au dépôt et à la diffusion de documents scientifiques de niveau recherche, publiés ou non, émanant des établissements d'enseignement et de recherche français ou étrangers, des laboratoires publics ou privés.

# The role of mixing in the large-scale ocean circulation

C. de Lavergne,<sup>1</sup> S. Groeskamp,<sup>2</sup> J. Zika,<sup>3</sup> H. L. Johnson<sup>4</sup>

<sup>1</sup>LOCEAN Laboratory, Sorbonne Université-CNRS-IRD-MNHN,  
Paris F-75005, France

<sup>2</sup>NIOZ Royal Netherlands Institute for Sea Research, P.O. Box 59, 1790 AB,  
Den Burg, Texel, The Netherlands

<sup>3</sup>School of Mathematics and Statistics, University of New South Wales,  
Sydney, Australia

<sup>4</sup>Department of Earth Sciences, University of Oxford,  
Oxford, United Kingdom

## 1 **Abstract**

2 Irreversible mixing of tracers and momentum in the ocean occurs via diffusion and friction at the  
3 scale of molecules. That such molecular processes profoundly influence basin-scale ocean cur-  
4 rents is counter-intuitive. Many successful theories of ocean circulation indeed ignore diffusive  
5 and frictional processes. Yet oceanographers have long recognized that turbulence can amplify  
6 irreversible mixing and its influence on large-scale flows. In recent years, substantial progress  
7 has been made in the mapping of mixing energized by three-dimensional and geostrophic tur-  
8 bulence. This progress not only helps to quantify connections between mixing and observed  
9 circulation systems, but also to better characterize these circulation systems. This chapter sur-  
10 veys the rapidly evolving understanding of the impacts of mixing on the strength and structure  
11 of major ocean gyres, overturning circulations and the Antarctic Circumpolar Current. Accu-  
12 mulating evidence suggests that global ocean circulation is shaped by energetic mixing near  
13 ocean boundaries, while either weak or largely adiabatic away from boundaries.

## 14 **Keywords**

15 Ocean circulation, currents, gyre, overturning, mixing, turbulence

## 1. Introduction

At low latitudes, the Earth receives more heat from the Sun than it radiates out to space over an annual orbit. The opposite occurs at high latitudes, where outgoing longwave radiation exceeds incoming shortwave insolation. This latitudinal contrast is the primary driving force of coupled atmosphere and ocean circulations. It is imprinted on the ocean surface, which gains heat at low latitudes and loses heat to the atmosphere at higher latitudes. This differential surface heating of the ocean generates and amplifies the contrast between warm tropical waters and colder waters that fill higher latitude and deep basins (Fig. 1). To counteract the tendency to warm warm waters and cool cold waters, the ocean must transfer heat from low to high latitudes.

Such transfer can be achieved by moving warm surface water into the region of surface heat loss, thus evacuating heat from the warm bowl and reducing exposure to cooling of the cold pool (Fig. 1a,b). This advective scenario implies a permanent or transient deformation or displacement of the warm bowl so that it stretches into the cooling latitudes. Compensating equatorward flow of colder waters can occur in the horizontal plane, establishing a horizontal circulation, such as a gyre or an eddy (Fig. 1a). Alternatively the compensating flow may take place in the vertical plane, leading to an overturning circulation, such as an inter-hemispheric overturning (Fig. 1b). By shifting water bodies along the meridional axis, horizontal and overturning circulations can thus mitigate the imbalance implied by the latitudinal contrast in surface heat fluxes.

The scenarios described above invoke exclusively advection (i.e., mass transport) and surface heat fluxes, implicitly assuming that the ocean interior is devoid of non-advective heat fluxes or is *adiabatic*. The opacity of seawater does prevent solar heating from penetrating significantly

deeper than 200 m. However, heat exchanges are not restricted to the sunlit surface layer. Through temperature diffusion or *mixing*, heat can be transferred between water bodies in the ocean interior. If diffusion is able to transfer heat from the warm bowl to the cold pool at a rate similar to the net low-latitude surface heat gain, the idealised two-layer ocean of Fig. 1 may achieve heat balance via mixing rather than circulation (Fig. 1c).

A recent calculation of mixing-induced heat transfer across temperature classes in a realistic ocean model finds that the peak transfer, estimated at 1.6 PW across the 22°C isotherm, is of similar magnitude to the peak poleward oceanic heat transport (Holmes et al. 2018a, 2019). This result suggests that mixing plays a central role in maintaining heat balance against differential surface heating. Does it imply that the diffusive scenario of Fig. 1c dominates over advective scenarios of Fig. 1a,b? The reality is more subtle, because advection and diffusion are not independent processes, and indeed combine to shape oceanic transports of mass and heat. For example, the presence of a diffusive heat supply to the cold pool may allow hemispheric overturning circulations to develop (Fig. 1d). These circulations depend upon the existence of mixing, and contribute to poleward heat transport.

Coupling between advection and diffusion is ubiquitous. Any mass transport that crosses iso-surfaces of a conservative tracer (e.g., surfaces of constant salinity) below the ocean surface requires mixing. Mixing of momentum also exerts a profound, direct influence on ocean currents. Conversely, mixing rates often depend on surrounding currents, and more specifically on the turbulent motions that stir the ocean. Indeed, over most of the ocean, turbulence elevates effective mixing rates well above the weak molecular diffusivities. Mass transports thus contribute to amplify mixing via turbulence. This implies that mixing and advection rely on shared sources of kinetic energy, ultimately derived from surface winds, surface buoyancy fluxes, tides,

and geothermal heating (Fig. 2). Understanding the role of mixing in global ocean circulation requires (i) quantifying mixing rates by tracking energy from external sources to turbulence to mixing, and (ii) identifying the upscale influence of turbulent mixing on large-scale current systems.

In this chapter, we will focus on current systems spanning thousands of kilometers: basin-scale ocean gyres, the Antarctic Circumpolar Current and subtropical and deep overturning circulations. We begin with an overview of mixing processes and their mathematical representation (section 2). We next examine features of the large-scale ocean circulation that can be understood without consideration of mixing (section 3). The discussion of the impacts of mixing focuses by turns on mechanisms (section 4), their distribution (section 5), and their consequences for observed overturning (section 6) and horizontal (section 7) circulations. The emerging view is that of a relatively adiabatic interior ocean circulation commanded by strongly mixing boundaries (section 8).

## 2. Flavours of mixing

Ocean flows are governed by the Navier-Stokes equations on a rotating sphere. The equations determine the evolution of the three-dimensional velocity vector  $\vec{u} = (u, v, w)$  as a function of inertial, pressure gradient, gravitational, Coriolis and frictional forces:

$$\frac{\partial \vec{u}}{\partial t} + \vec{u} \cdot \nabla \vec{u} = -\frac{1}{\rho} \nabla p + \vec{g} - f \vec{z} \times \vec{u} + \nabla \cdot \nu \nabla \vec{u} \quad (1)$$

where we have made the traditional approximation; that is, we neglected the vertical component of the Coriolis force. In (1),  $p$  is pressure,  $\rho$  density,  $\vec{g}$  the gravity vector,  $f$  the Coriolis parameter,  $\vec{z}$  the vertical unit vector,  $\nu$  the molecular kinematic viscosity of seawater, and  $\nabla$  the three-

dimensional gradient operator. The last term represents the divergence of the down-gradient momentum transfer achieved by frictional interactions between water molecules. Assuming no sources and sinks of momentum at ocean boundaries, it can be shown that this term leaves the average momentum over the whole ocean volume unchanged but decreases the global variance of momentum. These two integral properties are fundamental characteristics of diffusion.

Equation (1) does not suffice to characterise the evolution of the fluid. It must be complemented by the continuity equation (expressing mass conservation), an equation of state relating density to pressure, temperature and salinity, and evolution equations for conservative temperature  $\Theta$  and absolute salinity  $S_A$  (McDougall 2003, McDougall et al. 2012). The latter two equations are analogous to that governing the evolution of an arbitrary tracer  $C$ ,

$$\frac{\partial C}{\partial t} + \vec{u} \cdot \nabla C = Q_C + \nabla \cdot \kappa_C \nabla C, \quad (2)$$

where  $Q_C$  encapsulates interior sources and sinks and  $\kappa_C$  is the molecular diffusivity of  $C$ . A conservative tracer has  $Q_C \equiv 0$ ; this is the case for conservative temperature (except for subsurface solar heating) and absolute salinity. Boundary fluxes of  $C$  enter as boundary conditions on the last term in (2). In the absence of such fluxes, this diffusion term preserves the domain average  $C$  and decreases the domain-wide variance of  $C$ . The reduction of variance can be illustrated with the idealised heat balance of Fig. 1c: diffusion acts to reduce the temperature contrast between the two layers, hence to diminish global temperature variance, whereas surface forcing acts in the opposite sense. More generally, boundary fluxes are the only means to increase global variance of a conservative tracer, implying that mixing and boundary fluxes are intrinsically tied in this variance competition (Walín 1977, 1982, Zika et al. 2015).

Can the diffusive terms  $\nabla \cdot \nu \nabla \vec{u}$ ,  $\nabla \cdot \kappa_\Theta \nabla \Theta$  and  $\nabla \cdot \kappa_{S_A} \nabla S_A$  affect the large-scale distribution

of momentum  $\vec{u}$ ? Molecular diffusion coefficients  $\nu$ ,  $\kappa_\Theta$  and  $\kappa_{S_A}$  vary little about respective values of  $1 \times 10^{-6}$ ,  $1.4 \times 10^{-7}$  and  $1.4 \times 10^{-9} \text{ m}^2 \text{ s}^{-1}$ . The characteristic time to diffuse a momentum anomaly from the surface to 4 km depth follows as  $(4000\text{m})^2/\nu = 16 \times 10^{12} \text{ s}$  or about 500,000 years. Equivalent timescales for heat and salt are respectively one and three order(s) of magnitude larger. It is immediately apparent that molecular diffusivities are far too weak to affect global circulation systems known to evolve on timescales of seasons to millennia. Scaling frictional and Coriolis terms in (1) further shows that, for a typical value of  $f \sim 10^{-4} \text{ s}^{-1}$ , the two terms are comparable at length scales of  $10^{-1} \text{ m}$ . Only at length scales smaller than 10 centimetres do molecular processes become considerable.

Using fast probes able to measure velocity and temperature variations at centimetre scale, it is possible to estimate the rate of molecular dissipation of kinetic energy  $(-\nu(\nabla\vec{u})^2)$  and temperature variance  $(-\kappa_\Theta(\nabla\Theta)^2)$  along a vertical cast in the ocean (Osborn and Cox 1972, Osborn 1978, Chapter 14). Such measurements show that the ocean is strewn with small patches of elevated shear and temperature microstructure (Gregg 1987). The magnitude and distribution of the measured micro-scale gradients cannot be explained by large-scale momentum and temperature variations: they arise from intermittent turbulent motions. These motions stir large-scale gradients and produce small-scale variance that is ultimately dissipated by molecular interactions. As a result, molecular dissipation of momentum and temperature variance is typically several orders of magnitude larger than would be expected in a laminar ocean (Gargett and Osborn 1981, Oakey 1982).

Stirring by motions of intermediate scale—between major currents spanning thousands of kilometres and molecular processes acting over centimetres—thus accelerates the downscale cascade of variance and amplifies the gradients upon which molecular viscosity and diffusivities



act. The ability of turbulence to amplify mixing becomes apparent in equations (1) and (2) when a Reynolds decomposition of variables into mean and fluctuating components is performed:  $\vec{u} = \overline{\vec{u}} + \vec{u}'$ ,  $C = \overline{C} + C'$ , and so on. The overbar indicates an average over spatio-temporal scales larger than those of turbulence. Evolution equations for the mean momentum and mean tracer become (Gill 1982)

$$\frac{\partial \overline{\vec{u}}}{\partial t} + \overline{\vec{u}} \cdot \nabla \overline{\vec{u}} = -\frac{1}{\rho} \nabla \overline{p} + \vec{g} - f \vec{z} \times \overline{\vec{u}} + \nabla \cdot \nu \nabla \overline{\vec{u}} - \overline{\vec{u}' \cdot \nabla \vec{u}'}, \quad (3)$$

$$\frac{\partial \overline{C}}{\partial t} + \overline{\vec{u}} \cdot \nabla \overline{C} = \overline{Q_C} + \nabla \cdot \kappa_C \nabla \overline{C} - \overline{\vec{u}' \cdot \nabla C'}. \quad (4)$$

The last terms in (3) and (4) imply that correlations between fluctuations in velocity and velocity (or tracer) gradients can modify the mean velocity (or tracer) tendency. Using the continuity equation under Boussinesq approximation  $\nabla \cdot \vec{u} = 0$ , and assuming turbulent fluxes can be modelled by down-gradient Fickian diffusion, the system of equations is closed with

$$\overline{\vec{u}' \cdot \nabla C'} = \nabla \cdot \overline{\vec{u}' C'} = \nabla \cdot (-\vec{K}_C \cdot \nabla \overline{C}) \quad (5)$$

and analogous relations for each component of the mean velocity vector. In (5), we introduced the (a priori unknown) turbulent diffusivity vector  $\vec{K}_C$ . In most oceanic conditions, each component of the turbulent diffusivity vector will exceed its molecular counterpart and molecular terms in (3) and (4) can be neglected. However, molecular processes are still necessary and operate to dissipate variance: it is via an increase of the gradients available to molecular diffusivities that stirring increases rates of irreversible mixing. The phrase *irreversible mixing* refers to mixing involving molecular interactions and diminishing the domain-wide variance, whereas *stirring* refers to a transfer of variance to smaller scales.

Equations (3)-(5) imply that the impact of mixing on mean ocean circulation depends on the magnitude of turbulent diffusivities. Key to estimating these diffusivities is an understanding of

the rate-controlling processes that transfer variance to dissipation scales. Two pivotal regimes of oceanic turbulence have been identified: three-dimensional or small-scale turbulence, and geostrophic turbulence. Three-dimensional turbulence, triggered by gravitational and shear instabilities, is active on scales of 1-100 m. It induces isotropic turbulent mixing rates that range from molecular levels to  $10\text{-}100\text{ m}^2\text{ s}^{-1}$ . Values above  $10^{-2}\text{ m}^2\text{ s}^{-1}$  occur mostly within surface and bottom boundary layers, where boundary conditions are immediately felt (Large et al. 1994, van Haren and Gostiaux 2012). Away from boundaries, moderate turbulence levels are largely sustained by the breaking of internal waves generated by tides (Fig. 3a,b; Kunze et al. 2006, Waterhouse et al. 2014, de Lavergne et al. 2020). Three-dimensional turbulence mixes tracers and momentum alike, although the isotropic diffusivities of momentum and tracers can differ (Gaspar et al. 1990).

Geostrophic turbulence consists of mesoscale eddies, with a typical diameter of 10-100 km and a baroclinic velocity structure that spans the whole water column. Most of these eddies are generated by baroclinic instability of the large-scale flow environment (Charney 1947, Eady 1949, McWilliams and Chow 1981). As opposed to three-dimensional turbulence, they stir background tracer gradients only along density surfaces in the ocean interior (Iselin 1939, McDougall et al. 2014), and horizontally near the surface, at estimated rates varying from about  $10\text{ to }10^4\text{ m}^2\text{ s}^{-1}$  (Fig. 3c,d; Klocker and Abernathey 2014, Cole et al. 2015, Groeskamp et al. 2020, Chapter 9). In the surface boundary layer and where tracer surfaces are not aligned with density surfaces, mesoscale eddies are thus able to produce finescale tracer variance (Klein et al. 1998). This variance is ultimately dissipated at molecular scale with the aid of background three-dimensional turbulence (Smith and Ferrari 2009, Naveira Garabato et al. 2016). The cooperation of mesoscale, small-scale and molecular processes thus contributes to the homogenization of all tracers along density surfaces. Density surfaces being called *isopycnals*, the

phrase *isopycnal mixing* is often used as a shorthand for this suite of processes.

Rates of isopycnal mixing are thought to be set by mesoscale stirring, rather than by three-dimensional turbulence (Chapter 9). Stirring rates by mesoscale eddies are typically seven orders of magnitude larger than isotropic diffusivities. Consequently, mixing by three-dimensional turbulence is usually referred to as *diapycnal mixing*: its contribution to mixing along isopycnals being overwhelmed by that of geostrophic turbulence, only the contribution to mixing across isopycnals is considered. Because diapycnal gradients are well approximated by vertical gradients except at boundaries, diapycnal mixing is also frequently referred to as *vertical mixing*. We instead use the phrase *isotropic mixing*, for it is the most general and physical description of mixing by small-scale turbulence (McDougall et al. 2014).

In addition to tracer stirring, geostrophic turbulence causes efficient lateral and vertical redistribution of horizontal momentum (Rhines and Holland 1979). Mathematically, these effects reside in the last term of equation (3). The lateral redistribution effect, termed Reynolds stress, is often modelled by down-gradient diffusion along geopotential surfaces (Munk 1950, Smith and McWilliams 2003). However, this diffusive representation of momentum fluxes is imperfect because mesoscale eddies can transfer momentum up-gradient and accelerate or rectify the large-scale flow (Harrison 1978, Rhines and Holland 1979). The vertical redistributive effect, called eddy form stress, has a profound effect on large-scale currents (Johnson and Bryden 1989, Olbers 1998): even though mesoscale eddies are unable to flux tracers across isopycnals, they are adept at transferring momentum across isopycnals via pressure fluctuations. The induced vertical momentum transfers may be represented as Fickian vertical mixing provided the diffusivity has an appropriate form (Rhines and Young 1982, Gent et al. 1995). However, they are more commonly represented and interpreted as an eddy-induced mass transport due to cor-

relations between mesoscale velocities and isopycnal layer thicknesses (Gent and McWilliams 1990, McDougall and McIntosh 2001).

The example of eddy form stress shows that the same physical process can have alternative diffusive and advective representations, illustrating the difficulty in defining mixing. Still, it is possible to distinguish processes that unambiguously contribute to irreversible mixing, and thereby dissipate whole-ocean kinetic energy and/or tracer variance. Reynolds and eddy form stresses exerted by geostrophic turbulence do not qualify: they communicate momentum via pressure gradient forces rather than molecular friction. By contrast, three-dimensional turbulence directly contributes to dissipate both kinetic energy and tracer variance. Similarly, tracer stirring by geostrophic eddies contributes to irreversible mixing by transferring variance down to dissipation scales. In the remainder of this chapter, we will reserve the word *mixing* for only those processes causing irreversible mixing, and discuss the role of such processes in basin-scale ocean circulation (sections 4-7). In the next section, we briefly expose ocean circulation theories that do *not* appeal to mixing.

### 3. Non-dissipative theories of ocean circulation

In 1992, a purposeful tracer release experiment at 300 m depth in the northeastern Atlantic showed that the isotropic diffusivity in the region's pycnocline is close to  $10^{-5} \text{ m}^2 \text{ s}^{-1}$  (Ledwell et al. 1993). Temperature microstructure in the stratified upper ocean indicates similar average rates of temperature mixing, despite integrating the additional contribution of geostrophic turbulence (Osborn and Cox 1972, Gregg 1987, Davis 1994). At the rate of  $10^{-5} \text{ m}^2 \text{ s}^{-1}$ , diffusive heat transfer over 1 km takes about 3,000 years: too slow to compete with surface heat forcing and heat transport by upper-ocean currents. These observations motivated—or justified a

214 posteriori—the neglect of molecular-scale dissipation in landmark models of ocean circulation.

### 215 *a. Ekman pumping*

216 The first such model is due to Sverdrup. Classical scaling of equation (1) shows that, away  
217 from the equator, ocean currents are close to geostrophic balance: pressure gradient and Cori-  
218 olis forces set horizontal velocities. Cross-differentiation of zonal and meridional geostrophic  
219 equations and use of continuity yields

$$\beta v = f \frac{\partial w}{\partial z} \quad (6)$$

220 where  $\beta = df/dy$ . Equation (6) states that poleward (equatorward) flow must be balanced by  
221 vertical stretching (squeezing) of fluid columns. Winds are a prominent force able to squeeze or  
222 stretch water columns: the curl of the surface wind stress  $\vec{\tau}$  generates a pumping velocity  $w_{Ek}$  at  
223 the base of the thin surface Ekman layer. Vertical integration of (6) from a depth  $h_0$  of assumed  
224 zero vertical motion up to the bottom of the Ekman layer (of thickness  $h_{Ek}$ ) gives Sverdrup's  
225 prediction for the meridional circulation,

$$\beta \int_{z=-h_0}^{z=-h_{Ek}} v dz = f w_{Ek} = f \nabla \times (\vec{\tau}/f) . \quad (7)$$

226 Relation (7), called Sverdrup balance, proved very powerful to explain the broad equatorward  
227 (poleward) flow of subtropical (subpolar) gyres (Fig. 4). In this model, depth-integrated currents  
228 are shaped by direct wind forcing. This forcing relies on the existence of molecular friction,  
229 necessary for winds to transfer momentum to an initially still ocean surface. Yet wind stress  
230 effectively occurs via pressure forces onto surface waves (Plant 1982), so that Ekman pumping  
231 and Sverdrup balance do not depend on viscosity.

232 Sverdrup balance is mute about the vertical structure of circulation and density in the ocean.

The three-dimensional circulation problem is particularly complex because surface buoyancy fluxes, interior density gradients and ocean currents all depend upon each other. A major advance owes to Luyten et al. (1983), who established an adiabatic theory for the large-scale currents and density structure of the ocean thermocline. They assumed that the thermocline consists of a few homogeneous isopycnal layers governed by geostrophic and hydrostatic balances (thus retaining the first three terms on the right-hand side of (1)). Specifying surface densities where Ekman pumping is downward, they tracked the depth of isopycnals and the transport along isopycnals, progressing from the isopycnals' outcrop locations toward the equator. Their theory, called the ventilated thermocline theory, successfully predicts certain key features of the thermocline. It suggests that, underneath the direct influence of surface forcing, the density structure and ventilation of the upper ocean are essentially controlled by Ekman pumping—and largely independent of mixing.

An adiabatic model of circulation in the deep ocean was championed a decade later by Toggweiler and Samuels (1993, 1995, 1998). They proposed that a large proportion of dense waters that fill the ocean deeper than about 2 km are drawn to the surface by Ekman upwelling in the Southern Ocean (Fig. 5). There, westerly winds drive a divergent northward Ekman transport, while a zonally unbounded channel at Drake Passage latitudes (0-2 km; 56-60°S) results in the selection of deeper waters as the mass replacement for the surface divergence (Toggweiler and Samuels 1995). Indeed, within this channel, the zonal mean longitudinal pressure gradient is zero, and so the net meridional geostrophic flow must also be zero. Numerical experiments with global ocean models further showed that the wind-driven upwelling of dense waters occurs along rising isopycnals (Fig. 5) and persists in the limit of zero mixing (Toggweiler and Samuels 1998, Wolfe and Cessi 2011). This implies that an inter-hemispheric overturning circulation, akin to that schematized in Fig. 1b, can exist without mixing: (i) gravitational sinking

at northern high latitudes carries dense waters into the deep ocean; (ii) geostrophic southward flow brings these waters to the Ekman divergence south of 50°S, where they are lifted up to the surface; (iii) surface density transformations and northward upper-ocean currents close the circulation.

#### *b. Momentum redistribution by geostrophic turbulence*

Sverdrup balance does not explain the closure of gyres, which occurs via a return flow focused along the western boundary of ocean basins (Fig. 4). This return flow was long thought to rely on lateral Reynolds stresses induced by the mesoscale eddy field (Munk 1950, Pedlosky 1996). Form stress exerted by sloping bottom topography has more recently been acknowledged as the principal force upsetting Sverdrup balance along western boundaries (Hughes and de Cuevas 2001). Realistic ocean models indicate that both variable topography and geostrophic turbulence contribute to alter the balance (7) and shape the depth-integrated flow of major gyres (Le Corre et al. 2020). The same applies to the momentum balance of the Antarctic Circumpolar Current (ACC), the World Ocean’s largest current which flows eastward in the latitude range 40-70°S (Fig. 4). There, bottom form stress due to topographic obstacles along the ACC path provides the sink of zonal momentum necessary to balance that imparted at the surface by westerly winds (Munk and Palmén 1951). In this balance, geostrophic turbulence plays an essential role by transferring momentum downward via eddy form stresses, connecting the surface source to the bottom sink of zonal momentum (Olbers 1998, Ferreira et al. 2005).

Momentum redistribution by geostrophic eddies plays a similarly essential role in the ocean’s overturning circulations. Surface wind and buoyancy forcing often produces relatively steep isopycnal slopes that are baroclinically unstable. Baroclinic instability then generates mesoscale

eddies that act to flatten out the isopycnals (Gent et al. 1995). The slumping of isopycnals occurs via an eddy-induced baroclinic circulation which generally opposes Ekman pumping velocities (Marshall 1997, Marshall et al. 2002, Doddridge et al. 2016). This circulation alters the shallow overturning cells that span the subtropical thermocline (Doddridge et al. 2016) as well as the deep overturning circulation (Marshall and Speer 2012). In particular, mesoscale eddies can induce southward isopycnal mass fluxes within the zonally continuous ACC (Marshall 1997, Marshall and Radko 2003), thus overcoming the constraint on upper ocean southward flow at Drake Passage latitudes suggested by Toggweiler and Samuels (1995). Nevertheless, simulations of the Southern Ocean including realistic topography and a rich eddy field suggest only weak southward crossing of the ACC via eddy-induced mass transport (Zika et al. 2012, Mazloff et al. 2013, Dufour et al. 2015).

Lateral and vertical stresses induced by geostrophic turbulence thus modulate the ocean's response to Ekman pumping and surface buoyancy fluxes, implying a role for the ocean's chaotic nature in setting its circulation and stratification. However, the theories outlined in this section include no explicit role for temperature and salinity modification by turbulent mixing. Instead, they rationalize many of the observed features of the ocean by invoking purely adiabatic dynamics, asserting a view of ocean circulation in step with the scenarios illustrated in Fig. 1a,b.

## **4. How can mixing shape circulation?**

### *a. By altering surface wind and buoyancy forcing*

The conceptual frameworks exposed in the previous section take the wind stress and surface buoyancy fluxes or surface densities as given. However, these surface boundary conditions,



essential drivers of ocean circulation, depend on mixing and on the circulation itself.

First, the wind stress is a function of the difference between the wind velocity vector above the sea surface and the oceanic surface velocity vector (Pacanowski 1987, Duhaut and Straub 2006). Vertical momentum mixing near the surface acts to reduce the ocean surface velocity, generally augmenting the wind stress.

Second, surface heat and freshwater fluxes depend upon the sea surface temperature (SST), which is profoundly affected by mixing in the surface boundary layer. For example, SST cooling by surface heat loss in winter is generally damped by isotropic mixing, which redistributes the heat loss over the depth of the surface mixed layer. More generally, a given air-sea heat (or freshwater) flux induces a change in the temperature (or salinity) of the ocean surface that is inversely proportional to the mixed layer depth (MLD). Mixing processes controlling the MLD and its evolution thus play a major role in establishing surface densities and surface buoyancy fluxes. These processes include both momentum mixing (which affects the shear of Ekman and other currents, which in turn influences turbulence and MLD) and temperature and salinity mixing by mesoscale, submesoscale and three-dimensional turbulence (see Chapters 4 and 8).

#### *b. By altering density gradients*

On horizontal scales exceeding several kilometers, and away from frictional boundary layers, the ocean is in near geostrophic and hydrostatic balances. Combined, these balances give the thermal wind relationship

$$f \frac{\partial u}{\partial z} = g \frac{\partial \rho}{\partial y}, \quad f \frac{\partial v}{\partial z} = -g \frac{\partial \rho}{\partial x} \quad (8)$$

showing that the vertical variation of horizontal velocities is controlled by horizontal density

gradients. This implies that isotropic mixing can change horizontal circulation by altering horizontal variations in density. For example, localized deepening and densification of the surface mixed layer via surface buoyancy loss and convective mixing can stimulate horizontal motion around the convective chimney. On the other hand, isopycnal mixing catalyzed by mesoscale eddies does not modify density except for effects related to the non-linearity of the equation of state (McDougall 1984), and is therefore less able to modify horizontal circulation. In general, salinity and temperature modifications that have compensating effects on density have no impact on circulation unless they influence surface buoyancy forcing. Mixing of passive tracers is equally neutral to circulation—unless it impacts phytoplankton concentrations and, via their modulation of albedo and light absorption, near-surface densities (Sweeney et al. 2005).

Mixing can also affect circulation by altering the vertical density distribution. The densest ocean waters are formed at the surface by heat and freshwater loss to the atmosphere and cryosphere. Their gravitational, ageostrophic sinking into the deep ocean relies on their higher density relative to underlying waters. This density difference (between newly formed dense waters and underlying waters) owes to the mixing of sinking waters with lighter waters en-route to the deep ocean. Mixing thus maintains relatively low densities in the deep ocean that sustain the downwelling of the densest waters. As incoming dense waters intrude below older waters, they drive a compensating upwelling of these older waters. This upwelling is often quantified by a diapycnal velocity  $\omega$ , related to the divergence of the mixing-driven density flux  $F$  (Nurser et al. 1999),

$$\omega = \frac{\partial F}{\partial \rho} . \quad (9)$$

Equation (9) states that local density loss due to a divergent density flux is balanced by upward advection of denser water—with the reverse true for a convergent density flux. The diapycnal velocity  $\omega$  may be a true Eulerian velocity, as required at steady state, or merely a down-

ward (upward) movement of the isopycnal due to local lightening (densification). Note that the term diapycnal upwelling (downwelling) is used when the velocity  $\omega$  is directed toward lighter (denser) layers, even though the orientation of the velocity may vary.

Vertical velocities induced by mixing can then set up horizontal circulations (Stommel 1958, Pedlosky 1992). Indeed, equation (6) shows that, if the vertical velocity varies in the vertical, meridional geostrophic flow is expected to balance the local squeezing or stretching. For example, Stommel (1958) proposed that widespread upwelling across the 2 km depth interface generates broad interior poleward motion at depths greater than 2 km. Pedlosky (1992) further demonstrated that longitudinal variations in the upwelling rate can cause the deep meridional flow to have a sheared, baroclinic structure.

### *c. By producing and consuming water masses*

In the above situation of gravitational sinking enabled by mixing-driven reductions in density at depth, a circulation is established between the surface source and the bottom sink of dense waters. This perspective can be generalized as follows. Mixing both produces and consumes water masses; that is, it adds and removes mass from given density classes. If the ocean stratification is statistically steady, isopycnal mass transports (i.e., circulation) must connect the sources and sinks of mass within each isopycnal layer. Reciprocally, for an isopycnal circulation to be maintained, mass must be added at the starting point of the circulation and removed at its finish point. The mass gains and losses of isopycnal layers, referred to as *density transformations* or *water-mass transformations*, can occur at the surface via surface buoyancy fluxes, at the bottom via geothermal heating, or in the remainder of the ocean via mixing (Groeskamp et al. 2019).

Were mixing absent, circulation across density classes would be restricted to boundaries. This restriction is best illustrated by examining circulation in a density-depth coordinate system (Nycander et al. 2007; Fig. 6). In this space, the adiabatic circulations of Luyten et al. (1983) and Toggweiler and Samuels (1998) reduce to downward and upward motions at fixed density (Fig. 6a). They can be contrasted with the simplified overturning circulation of Munk and Wunsch (1998), whereby low-latitude upwelling from 4 to 1 km depth is enabled by mixing-driven buoyancy gain (Fig. 6b). By causing density transformations throughout the ocean volume, mixing thus confers an additional degree of freedom on the circulation. Whether observed overturning circulations are closer to the idealized scenarios of Figs. 1b and 6a, versus those of Figs. 1d and 6b, remains a matter of debate. We will argue that a more faithful depiction of the overturning involves a substantial decrease of density during the descent of dense waters, a modest decrease during their ascent along the seafloor, and upwelling at constant density from 2.5 km depth to the near surface (Fig. 6d).

## 5. Where is mixing most effective at shaping circulation?

The forces that set the ocean in motion (Fig. 2) and the mechanisms identified in section 4 hint at the locations where mixing is most influential on circulation: near the surface, and near the bottom. Here we briefly survey observed distributions of isotropic mixing and mesoscale stirring to substantiate this proposal. We define the near-surface region as waters shallower than the local annual maximum MLD plus 100 m, and the near-bottom region as waters lying within 500 m of the seafloor. The intervening waters will be referred to as the ocean interior. Thus defined, the ocean interior makes up 83% of the global ocean volume.

### *a. Isotropic mixing, from top to bottom*

The canonical pycnocline isotropic diffusivity of  $10^{-5} \text{ m}^2 \text{ s}^{-1}$  is usually deemed too small to be a leading-order control of circulation and tracer budgets (Ledwell et al. 1993, Davis 1994, Munk and Wunsch 1998). To evaluate this expectation, we apply a uniform mixing rate of  $10^{-5} \text{ m}^2 \text{ s}^{-1}$  to the observed density distribution (Figs. 5 and 7; Gouretski and Koltermann 2004), and deduce diapycnal velocities according to equation (9). By summing these velocities along isopycnals within each ocean basin, we obtain diapycnal mass transports (Fig. 8a), measured in Sverdrups (Sv;  $1 \text{ Sv} \equiv 10^6 \text{ m}^3 \text{ s}^{-1}$ ). The density measure employed from here on is the neutral density of Jackett and McDougall (1997) which does not depend on a reference pressure. The uniform  $10^{-5} \text{ m}^2 \text{ s}^{-1}$  mixing rate generates a few Sv of diapycnal upwelling within the 25.5-28  $\text{kg m}^{-3}$  density range, and a few Sv of downwelling at lower densities (Fig. 8a). Given that deep and subtropical overturning circulations are thought to carry a few tens of Sv (Ganachaud and Wunsch 2000, Lumpkin and Speer 2007), we conclude that an average diffusivity one order of magnitude larger, i.e.  $10^{-4} \text{ m}^2 \text{ s}^{-1}$ , would be required to make isotropic mixing a leading-order contributor to these circulations (Munk and Wunsch 1998).

Caveats to the above conclusion include (i) the dependence of diapycnal transports on the three-dimensional distribution of density and diffusivity (a uniform diffusivity causes different transports than a varying diffusivity with the same average) and (ii) the role of diffusivity in shaping the ocean's density distribution, which was taken as given. Nevertheless, the calculation provides a useful rule of thumb: regions where isotropic mixing plays a direct and substantial role in circulation are likely to have average diffusivities close to or larger than  $10^{-4} \text{ m}^2 \text{ s}^{-1}$ .

Winds and waves maintain high levels of mixing in the surface boundary layer (Chapter 4). Typically, this layer extends over a few tens to hundreds of meters, possesses quasi homogeneous properties and isotropic mixing rates in excess of  $10^{-2} \text{ m}^2 \text{ s}^{-1}$  (Gaspar et al. 1990, Large et al.

1994, de Boyer Montégut et al. 2004). When the ocean surface loses buoyancy, mixing rates are further enhanced by convective instability. Convection leads to deepening and density gain of the mixed layer (Fig. 6c), and underpins much of the pronounced seasonal cycle of MLD. Together, these surface mixing processes shape global ocean circulation and stratification by modifying surface currents and wind stresses, SST and air-sea buoyancy exchanges, as well as water-mass transformation and subduction. In particular, winter convective mixing plays a primary role in setting the properties of water masses entering and establishing the ocean's permanent stratification (Iselin 1939, Stommel 1979).

Energetic three-dimensional turbulence often encroaches below the base of the mixed layer. Turbulence may be triggered by pronounced vertical shear in the mean currents, as occurs in the shallow thermocline (near 50 m depth) of the central and eastern equatorial Atlantic and Pacific (Gregg et al. 1985, Smyth and Moum 2013, Hummels et al. 2013, Chapter 10). These mixing hotspots are outstanding: the shear of large-scale and mesoscale currents below the mixed layer is generally insufficient to set off such instabilities, particularly in the more sluggish ocean interior (Wunsch 1997). Storm-induced inertial oscillations of the mixed layer produce shear and mixing at its base (Pollard et al. 1973, Price et al. 1986, Chapter 5). In addition, these oscillations often radiate internal waves able to catalyze mixing deeper down (Alford and Gregg 2001, Jing and Wu 2014). In mid-latitude oceans, a consequent wintertime increase of the average isotropic diffusivity by up to an order of magnitude is observed down to 2 km depth (Whalen et al. 2018). Nonetheless, the wintertime diffusivity averaged over a large region remains of order  $10^{-5} \text{ m}^2 \text{ s}^{-1}$  (Whalen et al. 2018, Chapter 5), except in near-surface waters where the bulk of the energy supply to mixing lies (Zhai et al. 2009, Alford 2020).

Tides constitute a leading source of three-dimensional turbulence outside mixed boundary lay-

ers (Munk 1997, Waterhouse et al. 2014, de Lavergne et al. 2019, Vic et al. 2019). When tidal currents flow over uneven seafloor, they generate internal waves called *internal tides* that propagate and fuel three-dimensional turbulence throughout the global ocean (Garrett and Kunze 2007, Chapter 6). Estimated mixing rates due to internal tides vary widely in the horizontal and vertical, from  $10^{-6} \text{ m}^2 \text{ s}^{-1}$  up to  $10^{-2} \text{ m}^2 \text{ s}^{-1}$  in localized hotspots (Polzin et al. 1997, Rudnick et al. 2003, Waterhouse et al. 2014). They were recently mapped over the global ocean using Lagrangian tracking of internal tide energy from sources to sinks, accounting for local and remote pathways to mixing (Fig. 3a,b; de Lavergne et al. 2020). A zonal average of the thus estimated tidal diffusivity, weighted by  $|\frac{\partial \rho}{\partial z}|$  so that mean values relate to density fluxes, shows a sharp increase near 2.5 km depth from order  $10^{-5} \text{ m}^2 \text{ s}^{-1}$  above to order  $10^{-4} \text{ m}^2 \text{ s}^{-1}$  below (Fig. 9a). The transition at 2.5 km corresponds to the typical depth to which topographic ridges rise (Fig. 7). This zonal mean distribution indicates that internal tides cannot account for average mixing rates nearing  $10^{-4} \text{ m}^2 \text{ s}^{-1}$  above the depth range of major ridges. Given the broad agreement of the mapped tidal diffusivity with available observations of internal wave-driven turbulence below 400 m (de Lavergne et al. 2020), we contend that breaking internal waves are unlikely to sustain large diapycnal flows between 400 m and 2.5 km depth.

High isotropic diffusivities deeper than 2.5 km do not necessarily imply large net diapycnal upwelling. This is because these diffusivities are sufficiently concentrated near the bottom (Fig. 9a,b) that they tend to homogenize abyssal waters, rather than lighten them by draining buoyancy from the upper ocean. Indeed, close to rough or steep topography where elevated diffusivities are observed, turbulence is bottom-intensified (Toole et al. 1994, Polzin et al. 1997). As a result, the downward buoyancy flux increases toward the seafloor, except in a thin bottom layer where it must dwindle to match the bottom boundary condition (Fig. 10b; St Laurent et al. 2001, de Lavergne et al. 2016, Ferrari et al. 2016). Bottom-enhanced turbulence thus generates

a dipole of density transformation: buoyancy gain along the seafloor, and buoyancy loss immediately above (Fig. 10c; see also Chapter 7). The bottom lightening is associated with diapycnal upwelling, whereas the overlying densification implies diapycnal downwelling. Consequently, there is a substantial degree of cancellation between upwelling and downwelling that diminishes the ability of abyssal mixing to maintain a large-scale overturning circulation (de Lavergne et al. 2016, Ferrari et al. 2016, McDougall and Ferrari 2017).

The dipole of density transformation also applies to the second major source of mixing at depth: downslope or constricted ocean currents carrying dense waters over sills or through straits (Fig. 10a; Polzin et al. 1996, Bryden and Nurser 2003). In these locations, bottom-intensified turbulence draws energy from the flow itself, lightening waters hugging the seafloor while densifying and entraining overlying waters. Sills and straits host some of the largest deep-ocean turbulence levels and diffusivities (Ferron et al. 1998, MacKinnon et al. 2008, Voet et al. 2014). The induced diapycnal transports, although localized and of both signs, are responsible for step changes in bottom ocean properties (Fig. 10d) and abyssal stratification following dense water pathways (Mantyla and Reid 1983, Bryden and Nurser 2003).

#### *b. Mesoscale stirring, from top to bottom*

The near surface is where stirring by geostrophic turbulence is expected to be most efficient at shaping circulation, for four reasons. First, the competition between variance input by surface tracer fluxes and variance removal by mixing on the global scale (section 2) implies that temperature, salinity and density contrasts tend to decrease with depth. Second, mesoscale stirring rates are surface-intensified (Fig. 3c; Ferreira et al. 2005, Cole et al. 2015, Groeskamp et al. 2017, Canuto et al. 2019). Third, isopycnal stirring near the surface can modify the mixed layer



478 heat budget and air-sea buoyancy forcing (Guilyardi et al. 2001, Hieronymus and Nycander  
479 2013). Last, geometry demands that eddy stirring transitions from isopycnal to along-boundary  
480 directions within diabatic boundary layers (Treguier et al. 1997, Ferrari et al. 2008, Chapter 9).  
481 Over the depth of the surface mixed layer, mesoscale eddies thus directly affect the density field  
482 via horizontal stirring (Danabasoglu et al. 2008).

483 Horizontal stirring by geostrophic turbulence in the surface mixed layer has an important influ-  
484 ence on the transformation and subduction of water masses in certain regions (Robbins et al.  
485 2000, Price 2001, Groeskamp et al. 2016), thus affecting circulation in the deeper ocean. At  
486 the very surface, mesoscale stirring exchanges water across gradients in air-sea fluxes, modu-  
487 lating these fluxes and the ocean heat balance without reliance on irreversible mixing, much  
488 as sketched in Fig. 1a. In practice, however, active three-dimensional turbulence colludes with  
489 surface buoyancy forcing to dissipate the density variance produced by mesoscale currents in  
490 the surface mixed layer. Horizontal stirring and isotropic mixing thus interact to shape surface  
491 water mass transformations.

492 Below the surface mixed layer, isopycnal mixing can also accomplish density transformations,  
493 due to the nonlinear dependence of density on temperature and pressure. There are two separate  
494 effects, cabbeling and the thermobaric effect, which arise due to the dependence of the thermal  
495 expansion coefficient on temperature and pressure, respectively (McDougall 1984). When mix-  
496 ing two water parcels with different temperatures, the mixed product is denser than the average  
497 of the two initial densities, a process known as cabbeling. Via this effect, isopycnal mixing can  
498 cause densification and attendant diapycnal downwelling. Thermobaricity, on the other hand,  
499 can cause both lightening and densification, and is active when water parcels move across a  
500 substantial pressure range. Hence, for isopycnal stirring to induce significant density trans-

501 formations, it must mix across relatively large temperature and pressure contrasts. The ACC,  
502 whose steep isopycnals coincide with strong eddy activity and contrasting water masses, is one  
503 such region. Calculations suggest that isopycnal diffusivities of order  $10^3 \text{ m}^2 \text{ s}^{-1}$  are sufficient  
504 to cause 5-10 Sv of downwelling in the ACC region (Figs. 11a and 13a,b; Iudicone et al. 2008,  
505 Klocker and McDougall 2010, Nycander et al. 2015, Groeskamp et al. 2016).

506 At the bottom boundary, mesoscale stirring again must follow the direction of topography rather  
507 than that of isopycnals (Greatbatch and Li 2000). Since isopycnals intersect the seafloor at right  
508 angles, due to the insulating boundary condition (Wunsch 1970), mesoscale stirring must have  
509 a diapycnal component along the bottom topography. This effect, and its coupling with smaller  
510 scale turbulence in the bottom boundary layer, has received little attention to date. Whether  
511 near-bottom mesoscale diffusivities are sufficiently large to substantially alter density transfor-  
512 mations in the deep ocean is presently unknown.

## 513 **6. Some impacts on basin-scale overturning circulation**

514 The role of mixing in basin-scale overturning circulations is discussed in this section, focusing  
515 on quantitative assessments of mixing-driven water mass transformations. We begin with the  
516 circulation of the densest ocean waters and move progressively toward lighter layers.

### 517 *a. Abyssal overturning cell*

518 Antarctic Bottom Water (AABW) is the densest global-scale water mass. It is produced around  
519 Antarctica, sinks along the Antarctic continental slope and spreads northward to fill most of the  
520 ocean deeper than 4 km (Orsi et al. 1999). The northward deepening and ultimate grounding of

density surfaces at these depths indicate that AABW becomes progressively lighter as it flows northward (Fig. 5). Once lighter than about  $28.1 \text{ kg m}^{-3}$ , it returns southward and ultimately upward in the Antarctic divergence (Toggweiler and Samuels 1993, Ganachaud and Wunsch 2000). This circulation loop is often referred to as the abyssal overturning.

What causes the lightening of AABW along its path? The first and principal cause is mixing at sills and straits (Bryden and Nurser 2003). A map of neutral density at the ocean bottom shows that the density of bottom waters decreases from  $28.4 \text{ kg m}^{-3}$  or more near Antarctica to  $28.1\text{-}28.15 \text{ kg m}^{-3}$  at the northern end of the Indian, Atlantic and Pacific basins (Fig. 10d). This decrease occurs in steps that coincide with narrow passages connecting sub-basins, implicating intense mixing within constricted or overflowing currents (Polzin et al. 1996, Orsi et al. 1999). The second major cause is bottom-intensified mixing by breaking internal waves (de Lavergne et al. 2016, Ferrari et al. 2016), principally internal tides (Ledwell et al. 2000, Vic et al. 2019, de Lavergne et al. 2020, Chapter 6). Using a realistic map of mixing fueled by internal tides (de Lavergne et al. 2020), we estimate that tidal mixing converts about 15 Sv of  $28.11\text{-}28.2 \text{ kg m}^{-3}$  waters into lighter  $28.05\text{-}28.11 \text{ kg m}^{-3}$  waters (Fig. 8b). Of this conversion, a third occurs in the Southern Ocean (south of  $32^\circ\text{S}$ ), 6 Sv in the Indo-Pacific and 4 Sv in the Atlantic. A third primary cause of AABW lightening is geothermal heating (Adcroft et al. 2001, Emile-Geay and Madec 2009). Incorporating the contribution of geothermal heat fluxes mapped by Lucazeau (2019) into diapycnal velocities along the seafloor, we calculate that geothermal heating augments the peak diapycnal upwelling by about 7 Sv globally (Fig. 8b). The bulk of this geothermal density transformation occurs in the wide Pacific basin and is focused around  $28.11$  and  $28.03 \text{ kg m}^{-3}$  densities, which cover a large fraction of the North Pacific and southeastern Pacific seafloor, respectively (Fig. 10d).

544 These three causes of AABW lightening are not equivalent. Mixing in constrictive passages  
545 accounts for most of the overall density contrast traversed by the abyssal overturning circula-  
546 tion. However, its contribution to AABW lightening is restricted to densities greater than 28.15  
547  $\text{kg m}^{-3}$ , and is reliant on the existence of the circulation itself. The peak diapycnal upwelling,  
548 which dictates the level of meridional flow reversal and the magnitude of the circulation, occurs  
549 at lighter densities and is largely driven by breaking internal waves and geothermal heating (de  
550 Lavergne et al. 2017). Hence, tidal mixing and geothermal heating are the actual engines of  
551 the circulation: they supply potential energy to the flow, whereas overflow mixing consumes  
552 the flow's potential energy (Huang 1999, Bryden and Nurser 2003). Still, overflow mixing pro-  
553 foundly affects the strength of the circulation by shaping the abyssal stratification, thus modify-  
554 ing internal wave-driven mixing and the upwelling rates induced by geothermal buoyancy gains  
555 (Emile-Geay and Madec 2009, de Lavergne et al. 2016).

556 An additional difference between geothermal heating and abyssal mixing must be underlined.  
557 Geothermal heating provides a net buoyancy gain, moving water toward lighter layers only  
558 (Fig. 6c). By contrast, abyssal mixing is dominated by bottom-intensified turbulence, which  
559 causes near-compensating gains and losses of buoyancy near the bottom (Fig. 6c). This com-  
560 pensation limits the ability of bottom-enhanced turbulence to drive a net circulation toward  
561 lighter layers. In particular, bottom-intensified turbulence can cause net densification of a deep  
562 water mass (de Lavergne et al. 2016), even at the basin scale, as obtained here in the 28.02-28.09  
563  $\text{kg m}^{-3}$  density range within the Atlantic (Fig. 8b).

564 Geothermal heating and bottom-enhanced turbulence share one important characteristic: they  
565 cause buoyancy gain only along the seafloor. As a result, the net buoyancy gain of a density  
566 layer depends closely on its access to the ocean floor (de Lavergne et al. 2016, 2017, Holmes

et al. 2018b). In turn, access to the seafloor is strongly constrained by the ocean’s geometry (Fig. 12): 85% of the seafloor area lies deeper than 2.5 km; 8% lies between 1 and 2.5 km depth. This peculiar depth distribution of the seafloor largely restricts AABW upwelling to depths greater than 2.5 km and densities greater than  $28 \text{ kg m}^{-3}$  (Figs. 7 and 8b; de Lavergne et al. 2017). Diapycnal upwelling persists between 1 and 2.5 km depth ( $27.5\text{-}28 \text{ kg m}^{-3}$ ), but remains relatively constant at a magnitude of a few Sv (Fig. 8b). In this depth range, seafloor area is scarce (Fig. 12), density surfaces are relatively flat at low and middle latitudes (Figs. 5 and 7) and the isotropic diffusivity is relatively uniform in the vertical (Figs. 3a and 9). Circulation thus essentially abides by the one-dimensional recipe of Munk (1966),

$$\omega(z) = K_\rho \frac{\partial^2 \rho}{\partial z^2} / \frac{\partial \rho}{\partial z} \approx \text{constant}, \quad (10)$$

noting that the (horizontally averaged) vertical velocity and diffusivity are an order of magnitude less than Munk originally proposed. The 1-2.5 km depth range, or equivalently the  $27.5\text{-}28 \text{ kg m}^{-3}$  neutral density range of the modern ocean, could therefore be named the “Munk regime”. This regime hosts a relatively weak and weakly divergent diapycnal circulation, in contrast to the underlying “topographic regime”, where circulation is shaped by basin geometry and near-bottom mixing (Fig. 12).

Would the abyssal overturning persist in the absence of mixing? The presence of geothermal heating implies that it should persist so long as dense AABW is produced around Antarctica. Everything else equal, the abyssal ocean would be expected to become very dense, almost homogeneous, and traversed by a relatively swift circulation necessary to balance the steady geothermal buoyancy gain (Emile-Geay and Madec 2009). The abyssal circulation would have a structure broadly similar to that observed—constrained by topography and wind-driven upwelling—but would cross a much smaller density range. This thought experiment suggests

that the primary impact of mixing along the AABW path is to reduce the density of bottom waters and to increase the abyssal stratification. These effects have global repercussions throughout the water column.

### *b. North Atlantic Deep Water circulation*

The second major source of dense water in today's ocean is situated in the subpolar North Atlantic. Deep convective mixing in the Labrador Sea forms small amounts of dense water that participate in regional circulation and ventilate the deep ocean, but contribute little to global overturning (Pickart and Spall 2007, Lozier et al. 2019). Denser North Atlantic Deep Water (NADW) overflows at the submarine ridges that connect Scotland, Iceland and Greenland (Dickson and Brown 1994). This relatively salty deep water mass then traverses the whole Atlantic, flows along and across the ACC and reaches the near surface at high southern latitudes (Talley 2013, Tamsitt et al. 2017). A sinuous return flow in the upper ocean closes the circulation (Gordon 1986, Talley 2013), usually referred to as the Atlantic meridional overturning circulation (AMOC).

The pole-to-pole journey of NADW is generally conceptualized as a largely adiabatic circulation (Toggweiler and Samuels 1998, Wolfe and Cessi 2011, Nikurashin and Vallis 2012). However, observation-based tracer and mass budgets suggest that NADW undergoes substantial mixing with overlying and underlying waters, both within and outside the Atlantic basin (Talley 2013, Naveira Garabato et al. 2014). Nordic overflows are the first and primary mixing hotspot, and cause NADW to considerably increase in volume while decreasing in density (Dickson and Brown 1994, Lumpkin and Speer 2003). This reduction of NADW's density is critical because the difference in density between AABW and NADW controls their respective

volumes of influence and the depth of the AMOC (Galbraith and de Lavergne 2019, Sun et al. 2020).

Mixing-driven density transformations further downstream in the Atlantic depend in large part on the depth of NADW and its proximity to rough topography. The bulk of the southward flow occurs at depths greater than 2 km between densities 28 and  $28.15 \text{ kg m}^{-3}$  (Fig. 7b; Cunningham et al. 2007, Talley 2013), while the bulk of the Atlantic seafloor area lies at depths greater than 3 km or densities above  $28.05 \text{ kg m}^{-3}$  (de Lavergne et al. 2017). A sizeable portion of NADW is thus subject to strong near-bottom diapycnal transports. In the western Atlantic south of  $45^\circ\text{N}$ , bottom-enhanced turbulence is expected to make NADW colder and denser on average, because AABW covers most of the seafloor and tends to monopolize buoyancy gain. The strongest mixing of NADW with denser AABW may occur within the low-latitude fracture zones that channel flow from the western to the eastern Atlantic (Polzin et al. 1996, Mercier and Speer 1998, Demidov et al. 2007). Outflow from these channels is dominated by NADW, so that NADW occupies the deep eastern Atlantic down to the bottom (Sarmiento et al. 2007, de Lavergne et al. 2017). Mixing and geothermal heating in the abyssal eastern Atlantic thus serve to convert some of the densest ( $> 28.11 \text{ kg m}^{-3}$ ) NADW into lighter deep water. This conversion contributes to the temperature shift of NADW transport observed across the equator (Friedrichs et al. 1994).

What is the net effect of these density transformations on NADW? Over the whole Atlantic between  $32^\circ\text{S}$  and  $60^\circ\text{N}$ , we estimate that the impact of tidal mixing is to make NADW more homogeneous: about 5 Sv of  $28.07\text{-}28.11 \text{ kg m}^{-3}$  water are produced at the expense of denser and lighter categories (Fig. 8b). We find little upwelling of NADW across the mid-depth stratification and into the northward flowing upper branch of the circulation: only about 1 Sv of

28-28.03 kg m<sup>-3</sup> water is converted into < 27.6 kg m<sup>-3</sup> water (Fig. 8b). The actual amount of NADW upwelling into the Atlantic pycnocline may be larger, notably due to non-tidal sources of mixing that may dominate near the basin's western boundary (Zhai et al. 2010, Clément et al. 2016). Nonetheless, presently estimated diapycnal transports back the notion that the vast majority of NADW is exported all the way to the Southern Ocean (Toggweiler and Samuels 1995, Gnanadesikan 1999, Talley 2013).

*c. Southern Ocean upwelling: adiabatic or diabatic?*

Deep waters flowing out of the Pacific, Indian and Atlantic basins are thought to upwell along the sloping isopycnals of the Southern Ocean (Fig. 5; Toggweiler and Samuels 1993, Marshall 1997, Sloyan and Rintoul 2001, Marshall and Speer 2012). This upwelling is generally called adiabatic in the sense that it is density preserving (see Chapter 12). However, the isopycnal flow crosses isotherms and isohalines (Zika et al. 2009, Naveira Garabato et al. 2016, Tamsitt et al. 2018). This implicates mixing, enhanced by geostrophic and small-scale turbulence, in the temperature and salinity modifications of deep waters along their isopycnal upwelling path.

Diapycnal upwelling in the ACC has been suggested to play a role in returning deep waters to the surface. The main supporting evidence comes from the observed rapid spreading of passive tracers across isopycnals in the Atlantic sector of the ACC (Naveira Garabato et al. 2007, Watson et al. 2013). Within this sector, the measured spreading rate is consistent with a mid-depth isotropic diffusivity of order 10<sup>-4</sup> m<sup>2</sup> s<sup>-1</sup>. Applied to the climatological stratification of the Southern Ocean, a uniform mixing rate of this magnitude would cause about 10 Sv of diapycnal upwelling south of 32°S (Fig. 8a). However, the actual diapycnal flow is most certainly only a fraction of this rate, because diapycnal tracer spreading is slower in less hilly



sectors of the ACC (Ledwell et al. 2011, Watson et al. 2013), and because the effective mixing rate of a passive tracer can far exceed the effective mixing of density (Mashayek et al. 2017). Indeed, passive tracers tend to hover in regions of weak flow, elevated mixing and reduced stratification near topographic obstacles (Mashayek et al. 2017). Microstructure observations of turbulence in the Scotia Sea suggest that the effective mixing rate of density is much weaker than the diffusivity inferred from passive tracer measurements (St Laurent et al. 2012, Sheen et al. 2013).

Diapycnal downwelling of deep waters is equally plausible. Observations indicate that energetic turbulence in the ACC is often bottom-intensified. If dominated by bottom-enhanced turbulence, isotropic mixing could cause a few Sv of net diapycnal downwelling of circumpolar deep waters (Melet et al. 2014, de Lavergne et al. 2016). Estimated diapycnal transports due to tidal mixing south of 32°S indicate that upwelling dominates but remains weak at densities less than 28.05 kg m<sup>-3</sup> (Fig. 8b). Net diapycnal downwelling may also arise from isopycnal mixing and the non-linearity of the equation of state (Iudicone et al. 2008, Klocker and McDougall 2010, Groeskamp et al. 2016). We estimate that cabbeling and thermobaricity combined cause diapycnal downwelling varying between 2 and 4 Sv at densities larger than 27.5 kg m<sup>-3</sup> in the Southern Ocean (Fig. 11b). This downwelling may act to shift the upwelling toward larger densities or to increase the northward flow of AABW.

Hence, net diapycnal flow of deep waters in the ACC is most likely an order of magnitude weaker than the overall upwelling rate, thought to be between 20 and 30 Sv (Lumpkin and Speer 2007, Naveira Garabato et al. 2014). Upwelling does become diapycnal near the surface, however: alongside surface buoyancy forcing, mixing by three-dimensional turbulence plays an essential role in the entrainment of deep waters into the surface mixed layer and the diabatic

closure of the Southern Ocean overturning (Gordon and Huber 1990, Iudicone et al. 2008, Abernathey et al. 2016, Evans et al. 2018).

*d. The return flow to the North Atlantic*

NADW formation is the conversion of about 15 Sv of water from the ventilated pycnocline (densities  $< 27.5 \text{ kg m}^{-3}$ ) into denser waters (Lumpkin and Speer 2003). The compensating conversion can occur either through mixing-driven upwelling at low and middle latitudes (Munk and Wunsch 1998) or through near-surface lightening in the Southern Ocean (Toggweiler and Samuels 1993). We estimate that isotropic mixing causes about 3 Sv of upwelling across the  $27.5 \text{ kg m}^{-3}$  isopycnal (Figs. 8b and 13c), while isopycnal mixing induces an opposite transport of similar magnitude (Figs. 11b and 13a,b). These estimates imply that the net mass gain of the ventilated pycnocline occurs almost exclusively near the surface at southern high latitudes (Gnanadesikan 1999). A return flow of about 15 Sv must therefore exist from the Antarctic source of light water ( $< 27.5 \text{ kg m}^{-3}$ ) to its sink in the northern North Atlantic.

The first stage of this return route is the formation of mode and intermediate waters on the northern side of the ACC. Mixing in the surface boundary layer and immediately below plays an essential role in the formation of these subantarctic waters (McCartney 1977, Sloyan and Rintoul 2001, Iudicone et al. 2008, Sloyan et al. 2010). Cabbeling has also been highlighted as an important contributor to the formation of intermediate waters (Urakawa and Hasumi 2012, Nycander et al. 2015, Groeskamp et al. 2016). Along the northern flank of the ACC, cold and fresh southern waters come close to warmer and saltier subtropical waters within an active mesoscale eddy field (Abernathey et al. 2010). We estimate that the resultant mixing along isopycnals forms about 2 Sv of intermediate water in the  $27.25\text{-}27.5 \text{ kg m}^{-3}$  range (Figs. 11b and

13a,b). This number is somewhat lower than previous estimates. We attribute the difference primarily to the suppression of mesoscale stirring by mean currents (Ferrari and Nikurashin 2010). This suppression effect, included in the employed map of mesoscale diffusivities (Groeskamp et al. 2020), limits the intensity of isopycnal mixing and associated density transformations in the upper kilometer of the ACC (Fig. 3c).

A large fraction of subducted subantarctic waters feeds the return branch of the AMOC (Schmitz 1995). In the subtropical North Atlantic, this return branch is dominated by near-surface waters that are about 15°C warmer than subantarctic waters (Schmitz and Richardson 1991). This implies that substantial warming and lightening must occur along the journey (Fig. 5). Inverse box models suggest that the bulk of this transformation occurs at low latitudes in the eastern Pacific and Atlantic and relies largely on isotropic mixing (Lumpkin and Speer 2003, Sloyan et al. 2003). Elevated mixing in the upper layers of the eastern equatorial Pacific could be an important contributor to diapycnal upwelling of subantarctic water (Gregg et al. 1985, Smyth and Moum 2013, Holmes et al. 2018a). However, it remains unclear whether observed mixing is sufficient to accommodate the required cold to warm conversion. Toggweiler et al. (2019a,b) hypothesize that most of the conversion is actually achieved by direct atmospheric forcing near eastern margins. They propose that the AMOC indirectly draws warm water westward in the Pacific and Atlantic, exposing cool subantarctic water to surface heating at the eastern end of the basins. Their mechanism is well illustrated by the schematic of Fig. 1b (equating the cold water exposed to heating in the south with subantarctic water exposed at eastern margins) and alleviates the requirement for strong low-latitude mixing beneath and across the thermocline.

#### *e. Shallow hemispheric cells*

In addition to the return branch of the AMOC, the upper ocean hosts several closed overturning cells. The most prominent cells inhabit the top few hundred meters of subtropical oceans. These subtropical cells involve subduction poleward of about  $20^\circ$  and upwelling near the equator, connected by poleward surface Ekman flow and equatorward subsurface geostrophic flow (Roemmich 1983, Luyten et al. 1983, McCreary and Lu 1994, McPhaden and Zhang 2002). Convective mixing due to surface buoyancy loss shapes the rates and patterns of subduction (Marshall and Nurser 1991, McCreary and Lu 1994, Qu et al. 2013), while shear-driven mixing above the equatorial undercurrent in the Pacific and Atlantic contributes to lighten and return to the surface the upwelling waters (Lu et al. 1998, Moum et al. 2009, Hummels et al. 2013). Overall, subsurface isotropic mixing plays a key role in regulating the net overturning transport, that is, the residual of opposing Ekman and eddy-driven circulations (Henning and Vallis 2004, Doddridge et al. 2016).

Perhaps more importantly, climate model experiments have shown that SSTs, MLDs and the vertical structure of the thermocline are sensitive to the representation of isotropic mixing rates in the low-latitude upper ocean (Jochum et al. 2013, Melet et al. 2016, Zhu and Zhang 2019, Hieronymus et al. 2019, Chapter 2). Mixing near the surface has a weighty influence on air-sea interactions (Moum et al. 2013, Jochum et al. 2013, Zhu and Zhang 2019), while mixing in the interior affects the heat content of the thermocline and heat transport by the AMOC (Melet et al. 2016, Holmes et al. 2019, Hieronymus et al. 2019). Hence, the direct impacts of mixing on the ocean's temperature distribution have ripple-like effects on circulation within the thermocline and beyond.

## **7. Some impacts on basin-scale horizontal circulation**

We define horizontal circulations as networks of zonal and meridional currents integrated over a chosen depth range. An overturning circulation generally has a signature in horizontal circulation: for example, the Gulf Stream participates in both the AMOC and in the North Atlantic gyre circulation. The impacts outlined in the previous section thus have counterparts for circulation in the horizontal plane. We expand below on the consequences of mixing for the large-scale horizontal flow of the upper ocean, the abyss and the ACC.

#### *a. Upper-ocean gyres*

Sverdrup balance (7) suggests that depth-integrated flow is controlled by the wind stress curl. Munk (1950) first tested this prediction using observed winds. He introduced an additional Reynolds stress term (able to accommodate concentrated boundary currents) and showed that the main wind patterns create cyclonic subpolar gyres and anticyclonic subtropical gyres that resemble observed upper-ocean currents. This finding demonstrated that Ekman pumping is a major determinant of gyre circulations in upper layers of the global ocean. It was a sign that other factors, such as buoyancy forcing and mixing, are less important.

When applying (7), Munk (1950) assumed that vertical motion vanishes near 1 km depth, so that squeezing and stretching of the ocean's top kilometer is set by Ekman pumping velocities at the base of the Ekman layer. Could deep vertical motion sustained by mixing and overturning alter the rates of squeezing and stretching that shape upper-ocean gyres? Ekman pumping velocities are of order  $10^{-6} \text{ m s}^{-1}$  or 30 m per year (Roquet et al. 2011). In Fig. 13, we map the velocity across the  $27.5 \text{ kg m}^{-3}$  isopycnal that is necessary to balance estimated mixing-driven density transformations. Diapycnal velocities reach values of order  $10^{-6} \text{ m s}^{-1}$  only in specific hotspots of water mass transformation or near the outcropping or incropping of the considered isopycnal.

Over the vast majority of the upper ocean, Ekman pumping is therefore expected to dominate, suggesting that mesoscale stirring and tidal mixing play only a small role in driving gyres via squeezing and stretching of the ventilated pycnocline.

Regional hotspots of water mass transformation can nonetheless have major local and remote impacts on upper-ocean gyres, mediated by changes in regional density structure and mass balance. For example, mixing in the Nordic overflows has a first-order influence on the horizontal upper-ocean circulation of the whole North Atlantic (Lumpkin and Speer 2003, Zhang et al. 2011). Large tidal mixing rates in the western Pacific and Indonesian archipelago impact the throughflow between—and the gyres within—Pacific and Indian basins (Koch-Larrouy et al. 2010, Sasaki et al. 2018). In general, impacts of mixing on the AMOC have repercussions for the basin-scale horizontal circulation of the upper ocean (Toggweiler et al. 2019b).

Mixing near the surface plays a direct and widespread role. Subtropical gyres are linked to subtropical overturning cells (McCreary and Lu 1994, Samelson and Vallis 1997) and are therefore influenced by near-surface mixing via the mechanisms described in section 6e. Subpolar gyres conform less to Sverdrup balance than their subtropical twins: they are more strongly influenced by nonlinear dynamics and surface buoyancy forcing (Bryan et al. 1995, Su et al. 2014, Le Corre et al. 2020). In the Southern Hemisphere, near-surface meridional density gradients are the leading control on the strength of subpolar gyres simulated by climate models (Wang and Meredith 2008). These gradients, primarily set by freshwater and heat exchanges with the atmosphere and cryosphere, are modulated by mixing (Pellichero et al. 2017, Thompson et al. 2018).

#### *b. The Stommel and Arons circulation*

Horizontal circulation patterns in the deep ocean have received comparatively little attention. The reference theory for these patterns was proposed sixty years ago by Stommel (1958) and Stommel and Arons (1959a,b). This theory is based on equation (6) integrated from the seafloor ( $z = -H$ ) to a chosen abyssal depth ( $z = -h_{top}$ ):

$$\beta \int_{z=-H}^{z=-h_{top}} v \, dz = f[w(z = -h_{top}) - w(z = -H)] . \quad (11)$$

Stommel (1958) reasoned that the production and sinking of cold waters near Greenland and Antarctica should be balanced by downward diffusion of heat and upwelling across stratification at lower latitudes. Using (11) and assuming that the upwelling velocity at 2 km depth exceeds that at the bottom, Stommel mapped mass transports below 2 km as broadly poleward except near western boundaries, where fast currents governed by different dynamics were assumed to close the mass balance.

The circulation patterns drawn by Stommel (1958) and Stommel and Arons (1959a,b) have been shown to hold in idealized flat-bottom model oceans where a deep overturning is maintained by downward diffusion of buoyancy at a uniform rate (Samelson and Vallis 1997). Observational inferences of deep circulation have invariably revealed a different and much more complex picture (Friedrichs and Hall 1993, Hautala and Riser 1993, Reid 1997, 2003). Reasons are manifold. First, the theory assumes that the deep ocean hosts divergent vertical motion everywhere away from sinking regions. In reality, the area-integrated upwelling rate of deep waters at low and middle latitudes increases with height only up to about 4 km depth, then decreases with height until about 2.5 km depth (Fig. 8b; de Lavergne et al. 2017). Meanwhile, the ocean area increases markedly, so that the area-averaged upwelling tends to be less divergent than its area-integrated counterpart (McDougall 1989, Rhines 1993). Hence, convergent vertical motion favoring equatorward flow may be more common than the reverse. Moreover, upwelling

is not horizontally uniform: it is a balance of upward and downward velocities that are largest near topography (Fig. 10). Bottom-intensified mixing entails complex patterns of squeezing and stretching that depend on local characteristics of topography and turbulence (St Laurent et al. 2001, McDougall and Ferrari 2017).

More importantly, horizontal flow in the abyss is strongly constrained by topography and is influenced by a range of dynamics not reflected in the combination of (9) and (11) (Holland 1978, Garrett 1991, Pedlosky 1992, Callies 2018, Naveira Garabato et al. 2019, Yang et al. 2020; see also Chapters 7 and 8). How mixing interacts with such dynamics to shape abyssal current systems is expected to vary between regions and remains little studied.

### *c. The Antarctic Circumpolar Current*

The ACC transports over 130 Sv eastward as it circumnavigates Antarctica (Fig. 4; Meredith et al. 2011). The current has its largest speeds at the surface, but extends down to the seafloor (Peña-Molino et al. 2014). It is deemed to be driven in large part by Southern Hemisphere westerly winds (Munday et al. 2011, Howard et al. 2014). Indeed, if the global ocean were mixed to a single temperature and salinity, a full-depth ACC would likely persist as a conduit between momentum input at the surface and removal into the solid earth.

Strong contrasts in temperature, salinity and density are actually observed across the ACC. The zonal mass transport of the ACC can therefore be decomposed into a depth-independent component equal to the bottom velocity and a depth-dependent component obtained by vertical integration of the thermal current shear (8). This second component is directly linked to the meridional density difference across the ACC and accounts for about 85% of the total eastward



transport (Peña-Molino et al. 2014). Any impact of mixing on meridional density gradients in the Southern Ocean thus has implications for the strength and vertical structure of the ACC.

For instance, larger background rates of isotropic mixing tend to lower isopycnals north of the ACC and thereby increase the thermal current shear and ACC transport (Munday et al. 2011). Likewise, deep convective mixing south of the ACC can enhance the north-south density gradient and accelerate the ACC (Behrens et al. 2016). Bottom-intensified mixing in the abyss has also been found to alter the ACC density structure and flow, in ways that depend on the latitudinal distribution of that mixing (Jayne 2009, Melet et al. 2014).

Isopycnal mixing may also affect the ACC strength. Diapycnal downwelling due to cabbeling and thermobaricity, by acting as a sink of volume for the ventilated pycnocline, could contribute to raising isopycnals north of the ACC and slowing the circumpolar flow. Furthermore, isopycnal mixing can alter air-sea interactions at high latitudes and, via the induced changes in wind stress, convection and stratification, modify the ACC (Ragen et al. 2020).

Mixing can further influence the ACC by changing the strength of the meridional overturning circulation, without necessarily changing meridional density gradients within the current. Indeed, cross-stream flows affect the zonal momentum balance of the ACC (Gent et al. 2001, Howard et al. 2014, Stewart and Hogg 2017). In particular, an increased abyssal overturning strength (such as may result from increased deep mixing) has the potential to accelerate the ACC as follows: the Coriolis force acts to deflect the northward AABW flow to the west, and the southward return flow to the east; the westward abyssal momentum is damped by topographic form stress and bottom friction; a net gain of depth-integrated eastward momentum ensues (Howard et al. 2014).

The vertical and zonal extent of the ACC makes it a crossroads of global ocean circulation (Rintoul and Naveira Garabato 2013, Chapter 12). The ACC's structure and intensity are consequently tied to water mass transformations in all parts of the World Ocean.

## 8. Conclusions

Munk (1966) first conjectured that mixing between water masses occurs mostly where these water masses meet the surface and the seafloor. Here we estimated that isotropic and isopycnal mixing in the ocean interior (defined as in section 5) gives rise to diapycnal circulations of only a few Sverdrups. Rates of basin-scale overturning are thought to be an order of magnitude larger (Ganachaud and Wunsch 2000, Lumkin and Speer 2007). This implies that Munk was right, and the diapycnal component of global ocean circulation is largely confined to near-surface and near-bottom regions. Although this notion is long established (Munk and Wunsch 1998, Wunsch and Ferrari 2004), its consequences for the structure of ocean circulation remain under-appreciated.

The first and foremost consequence of boundary-intensified mixing is the organization of circulation by outcrop and incrop areas—that is, by the access of water masses to boundary regions. Three main regimes can be identified (Fig. 12): (i) a ventilated pycnocline where air-sea exchanges and mixing near surface outcrops govern the structure and rate of circulation; (ii) a topographic regime where abundant seafloor deeper than 2.5 km leads to substantial near-bottom density transformations; and (iii) an intervening Munk regime, more isolated from boundaries, where interior mixing maintains a modest diapycnal circulation. In the topographic regime, circulation is both strong and strongly influenced by near-bottom mixing. In the Munk regime, basin-averaged circulation and isotropic mixing rates are relatively weak (Figs. 7-9). In the ven-

876 tilted pycnocline, circulation is strong and strongly influenced by mixing near the surface, yet  
877 largely along-isopycnal in the interior.

878 A related consequence is the relationship between seafloor geometry and overturning circula-  
879 tion. Munk and Wunsch (1998), in their calculation of the effective diffusivity needed to upwell  
880 dense waters from 4 km to 1 km depth, did not account for the change with depth of the ocean's  
881 area. Actually, the small change of the ocean's area between 1 and 2.5 km depth impedes near-  
882 boundary diapycnal upwelling, whereas its rapid decrease at greater depths allows large diapy-  
883 cnal transports (de Lavergne et al. 2017). The depth distribution of the seafloor thus places a  
884 primary constraint on the structure of the overturning circulation. The compartmentalization of  
885 the deep ocean into subbasins connected by sills and straits exerts an additional and essential  
886 constraint (Bryden and Nurser 2003). A third crucial geometric ingredient is the interruption  
887 of north-south continental barriers in the Southern Ocean, which favours deep southward flow  
888 across the ACC (Toggweiler and Samuels 1995). Combined, these three ingredients lead to  
889 the simplified depiction in density-depth space of a bathymetrically constrained overturning  
890 (Fig. 6d).

891 Both NADW and AABW undergo larger density losses during their descent than their ascent,  
892 and both benefit from isopycnal Southern Ocean upwelling to come back to the surface (Fig. 6d).  
893 Differences between the abyssal overturning cell and the AMOC do nevertheless exist. The  
894 abyssal overturning cell inhabits the topographic regime and can be considered essentially di-  
895 abatic, in that its existence relies on the lightening of AABW at depth (Nikurashin and Vallis  
896 2012). NADW is partially embedded in the topographic regime and undergoes substantial trans-  
897 formation by near-bottom mixing (section 6b). However, density losses that are essential to the  
898 closure of the AMOC are believed to occur near the surface at southern high latitudes (Tog-

gweiler and Samuels 1998, Marshall and Speer 2012) and at low latitudes (Toggweiler et al. 2019a,b). The AMOC may thus be considered as more adiabatic, insofar as its existence and structure depend less on mixing below the near-surface region.

We posited that mixing in the ocean interior has less of an influence on circulation than near-boundary mixing, because it causes comparatively weak diapycnal flows. However, interior mixing does impact circulation in several indirect and important ways. In particular, isopycnal mixing catalyzed by mesoscale eddies modifies the temperature and salinity of water masses within the ocean interior. These modifications then affect air-sea interactions where the modified water masses outcrop (Guilyardi et al. 2001, Hieronymus and Nycander 2013, Ragen et al. 2020). In addition, weak rates of isotropic mixing in the voluminous ocean interior exert an important influence on the stratification and heat balance of the upper ocean (Melet et al. 2016, Holmes et al. 2018a, Hieronymus et al. 2019). Altered density and temperature distributions then impact the structure and strength of horizontal and overturning circulations (Sasaki et al. 2018, Zhu and Zhang 2019).

Mixing in the ocean interior is also essential for ventilation—that is, for the circulation of tracers (rather than the circulation of mass, which is the subject of this chapter). Tracer distributions are influenced by mixing via the impacts of mixing on ocean currents, but they are also directly impacted by mixing. These direct impacts are tracer specific, since diffusive tracer fluxes depend on tracer gradients in addition to diffusivities. For example, small isotropic diffusivities can cause weak buoyancy fluxes but large tracer fluxes. Weak mixing rates in the ocean interior can thus maintain important diapycnal tracer fluxes even in the absence of a diapycnal circulation. Furthermore, isopycnal mixing in the interior plays a key role in shaping global tracer distributions (Ledwell et al. 1998, Jones and Abernathy 2019) and is able to dominate over

ventilation by the large-scale mean currents (Holzer and Primeau 2006, Naveira Garabato et al. 2017). As such, interior mixing participates in setting the global state of climate and marine ecosystems in multiple and often underrated ways.

Understanding how circulation and mixing together establish the pathways and timescales of ocean ventilation constitutes a major and central challenge to this day. The recent advent of global three-dimensional maps of isotropic and isopycnal diffusivities (Fig. 3) opens up avenues for headway. However, these maps are incomplete and insufficiently constrained. New field measurements, coupled with research into the physics and energetics of turbulence across scales, are called for to incorporate all leading-order processes into comprehensive and realistic maps. Mechanistic understanding of the energy routes from forcing to circulation to mixing is essential to construct models that not only capture the observed mixing distributions, but also evolve these distributions consistently with changing boundary conditions (Eden et al. 2014). The path to faithful, conservative representation of the energy cycle (Fig. 2) in ocean models is long but vital to confidently probe and project ocean ventilation and its role in the climate system.

## References

- Abernathey, R., Marshall, J., Mazloff, M., Shuckburgh, E., 2010. Enhancement of mesoscale eddy stirring at steering levels in the Southern Ocean. *J. Phys. Oceanogr.* 40, 170–184.
- Abernathey, R.P., Cerovecki, I., Holland, P.R., Newsom, E., Mazloff, M., Talley, L.D., 2016. Water-mass transformation by sea ice in the upper branch of the Southern Ocean overturning. *Nature Geoscience* 9, 596–601.
- Adcroft, A., Scott, J.R., Marotzke, J., 2001. Impact of geothermal heating on the global ocean circulation. *Geophysical Research Letters* 28, 1735–1738.

- 945 Alford, M.H., Gregg, M.C., 2001. Near-inertial mixing: Modulation of shear, strain and mi-  
946 crostructure at low latitude. *J. Geophys. Res.* 106, 16947–16968.
- 947 Alford, M.H., 2020. Revisiting near-inertial wind-work: Slab models, relative stress, and mixed  
948 layer deepening. *J. Phys. Oceanogr.* 50, 3141–3156.
- 949 Behrens, E., Rickard, G., Morgenstern, O., Martin, T., Osprey, A., Joshi, M., 2016. Southern  
950 Ocean deep convection in global climate models: A driver for variability of subpolar gyres  
951 and Drake Passage transport on decadal timescales. *J. Geophys. Res.* 121, 3905–3925.
- 952 Bessières, L., Madec, G., Lyard, F., 2008. Global tidal residual mean circulation: Does it affect  
953 a climate OGCM? *Geophysical Research Letters* 35, L03609.
- 954 Bryan, F.O., Böning, C.W., Holland, W.R., 1995. On the midlatitude circulation in a high-  
955 resolution model of the North Atlantic. *J. Phys. Oceanogr.* 25, 289–305.
- 956 Bryden, H.L., Nurser, A.J.G., 2003. Effects of strait mixing on ocean stratification. *J. Phys.*  
957 *Oceanogr.* 33, 1870–1872.
- 958 Callies, J., 2018. Restratification of abyssal mixing layers by submesoscale baroclinic eddies.  
959 *J. Phys. Oceanogr.* 48, 1995–2010.
- 960 Canuto, V.M., Cheng, Y., Howard, A.M., Dubovikov, M.S., 2019. Three-Dimensional, space-  
961 dependent mesoscale diffusivity: Derivation and implications. *J. Phys. Oceanogr.* 49,  
962 1055–1074.
- 963 Charney, J.G., 1947. The dynamics of long waves in a baroclinic westerly current. *J. Meteor.*  
964 4, 136–162.
- 965 Clément, L., Frajka-Williams, E., Sheen, K.L., Brearley, J.A., Naveira Garabato, A.C., 2016.  
966 Generation of internal waves by eddies impinging on the western boundary of the North  
967 Atlantic. *J. Phys. Oceanogr.* 46, 1067–1079.
- 968 Cole, S.T., Wortham, C., Kunze, E., Owens, W.B., 2015. Eddy stirring and horizontal diffusiv-  
969 ity from Argo float observations: Geographic and depth variability. *Geophysical Research*

Letters 42, 3989–3997.

Cunningham, S.A., Kanzow, T., Rayner, D., Baringer, M.O., Johns, W.E., Marotzke, J., Longworth, H.R., Grant, E.M., Hirschi, J.J.-M., Beal, L.M., Meinen, C.S., Bryden, H.L., 2007. Temporal variability of the Atlantic meridional overturning circulation at 26.5°N. *Science* 317, 935–938.

Danabasoglu, G., Ferrari, R., McWilliams, J.C., 2008. Sensitivity of an ocean general circulation model to a parameterization of near-surface eddy fluxes. *J. Climate* 21, 1192–1208.

Davis, R.E., 1994. Diapycnal mixing in the ocean: The Osborn–Cox Model. *J. Phys. Oceanogr.* 24, 2560–2576.

de Boyer Montégut, C., Madec, G., Fischer, A.S., Lazar, A., Iudicone, D., 2004. Mixed layer depth over the global ocean: An examination of profile data and a profile-based climatology. *J. Geophys. Res.* 109, C12003.

de Lavergne, C., Falahat, S., Madec, G., Roquet, F., Nycander, J., Vic, C., 2019. Toward global maps of internal tide energy sinks. *Ocean Modelling* 137, 52–75.

de Lavergne, C., Madec, G., Le Sommer, J., Nurser, A.J.G., Naveira Garabato, A.C., 2016. On the consumption of Antarctic Bottom Water in the abyssal ocean. *J. Phys. Oceanogr.* 46, 635–661.

de Lavergne, C., Madec, G., Roquet, F., Holmes, R.M., McDougall, T.J., 2017. Abyssal ocean overturning shaped by seafloor distribution. *Nature* 551, 181–186.

de Lavergne, C., Vic, C., Madec, G., Roquet, F., Waterhouse, A.F., Whalen, C.B., Cuypers, Y., BouruetAubertot, P., Ferron, B., Hibiya, T., 2020. A parameterization of local and remote tidal mixing. *Journal of Advances in Modeling Earth Systems* 12, e2020MS002065.

Demidov, A.N., Dobrolyubov, S.A., Morozov, E.G., Tarakanov, R.Y., 2007. Transport of bottom waters through the Vema Fracture Zone in the Mid-Atlantic ridge. *Dokl. Earth Sc.* 416, 1120–1124.

995 Dickson, R.R., Brown, J., 1994. The production of North Atlantic Deep Water: Sources, rates,  
 996 and pathways. *J. Geophys. Res.* 99, 12319–12341.

997 Doddridge, E.W., Marshall, D.P., Hogg, A.McC., 2016. Eddy cancellation of the Ekman cell in  
 998 subtropical gyres. *J. Phys. Oceanogr.* 46, 2995–3010.

999 Dufour, C.O., Griffies, S.M., de Souza, G.F., Frenger, I., Morrison, A.K., Palter, J.B., Sarmiento,  
 1000 J.L., Galbraith, E.D., Dunne, J.P., Anderson, W.G., Slater, R.D., 2015. Role of mesoscale  
 1001 eddies in cross-frontal transport of heat and biogeochemical tracers in the Southern Ocean. *J.*  
 1002 *Phys. Oceanogr.* 45, 3057–3081.

1003 Duhaut, T.H.A., Straub, D.N., 2006. Wind stress dependence on ocean surface velocity: Impli-  
 1004 cations for mechanical energy input to ocean circulation. *J. Phys. Oceanogr.* 36, 202–211.

1005 Eady, E.T., 1949. Long waves and cyclone waves. *Tellus* 1, 33–52.

1006 Eden, C., Czeschel, L., Olbers, D., 2014. Toward energetically consistent ocean models. *J.*  
 1007 *Phys. Oceanogr.* 44, 3160–3184.

1008 Emile-Geay, J., Madec, G., 2009. Geothermal heating, diapycnal mixing and the abyssal circu-  
 1009 lation. *Ocean Science* 5, 203–217.

1010 Evans, D.G., Zika, J.D., Garabato, A.C.N., Nurser, A.J.G., 2018. The cold transit of Southern  
 1011 Ocean upwelling. *Geophysical Research Letters* 45, 13386–13395.

1012 Ferrari, R., Mashayek, A., McDougall, T.J., Nikurashin, M., Campin, J.-M., 2016. Turning  
 1013 ocean mixing upside down. *J. Phys. Oceanogr.* 46, 2239–2261.

1014 Ferrari, R., McWilliams, J.C., Canuto, V.M., Dubovikov, M., 2008. Parameterization of eddy  
 1015 fluxes near oceanic boundaries. *J. Climate* 21, 2770–2789.

1016 Ferrari, R., Nikurashin, M., 2010. Suppression of eddy diffusivity across jets in the Southern  
 1017 Ocean. *J. Phys. Oceanogr.* 40, 1501–1519.

1018 Ferreira, D., Marshall, J., Heimbach, P., 2005. Estimating eddy stresses by fitting dynam-  
 1019 ics to observations using a residual-mean ocean circulation model and its adjoint. *J. Phys.*



1020 Oceanogr. 35, 1891–1910.

1021 Ferron, B., Mercier, H., Speer, K., Gargett, A., Polzin, K., 1998. Mixing in the Romanche  
1022 fracture zone. *J. Phys. Oceanogr.* 28, 1929–1945.

1023 Friedrichs, M.A.M., Hall, M.M., 1993. Deep circulation in the tropical North Atlantic. *Journal*  
1024 *of Marine Research* 51, 697–736.

1025 Friedrichs, M.A.M., McCartney, M.S., Hall, M.M., 1994. Hemispheric asymmetry of deep  
1026 water transport modes in the western Atlantic. *J. Geophys. Res.* 99, 25165–25179.

1027 Galbraith, E., de Lavergne, C., 2019. Response of a comprehensive climate model to a broad  
1028 range of external forcings: relevance for deep ocean ventilation and the development of late  
1029 Cenozoic ice ages. *Climate Dynamics* 52, 653–679.

1030 Ganachaud, A., Wunsch, C., 2000. Improved estimates of global ocean circulation, heat trans-  
1031 port and mixing from hydrographic data. *Nature* 408, 453–457.

1032 Gargett, A.E., Osborn, T.R., 1981. Small-scale shear measurements during the fine and mi-  
1033 crostructure experiment (Fame). *J. Geophys. Res.* 86, 1929–1944.

1034 Garrett, C., 1991. Marginal mixing theories. *Atmosphere-Ocean* 29, 313–339.

1035 Garrett, C., Kunze, E., 2007. Internal tide generation in the deep ocean. *Annual Review of*  
1036 *Fluid Mechanics* 39, 57–87.

1037 Gaspar, P., Grégoris, Y., Lefevre, J.-M., 1990. A simple eddy kinetic energy model for simula-  
1038 tions of the oceanic vertical mixing: Tests at station Papa and Long-Term Upper Ocean Study  
1039 site. *J. Geophys. Res.* 95, 16179–16193.

1040 Gent, P.R., Large, W.G., Bryan, F.O., 2001. What sets the mean transport through Drake Pas-  
1041 sage? *J. Geophys. Res.* 106, 2693–2712.

1042 Gent, P.R., McWilliams, J.C., 1990. Isopycnal mixing in ocean circulation models. *J. Phys.*  
1043 *Oceanogr.* 20, 150–155.

1044 Gent, P.R., Willebrand, J., McDougall, T.J., McWilliams, J.C., 1995. Parameterizing eddy-

1045 induced tracer transports in ocean circulation models. *J. Phys. Oceanogr.* 25, 463–474.

1046 Gill, A.E., 1982. *Atmosphere–Ocean Dynamics*. Elsevier.

1047 Gnanadesikan, A., 1999. A simple predictive model for the structure of the oceanic pycnocline.

1048 *Science* 283, 2077–2079.

1049 Gordon, A.L., 1986. Inter-ocean exchange of thermocline water. *J. Geophys. Res.* 91, 5037–5046.

1050 Gordon, A.L., Huber, B.A., 1990. Southern ocean winter mixed layer. *J. Geophys. Res.* 95,

1051 11655.

1052 Gouretski, V., Koltermann, K.P., 2004. WOCE Global Hydrographic Climatology. *Berichte des*

1053 *BSH* 35, 1–52.

1054 Greatbatch, R.J., Li, G., 2000. Alongslope mean flow and an associated upslope bolus flux of

1055 tracer in a parameterization of mesoscale turbulence. *Deep Sea Research* 47, 709–735.

1056 Gregg, M.C., 1987. Diapycnal mixing in the thermocline: A review. *J. Geophys. Res.* 92,

1057 5249.

1058 Gregg, M.C., Peters, H., Wesson, J.C., Oakey, N.S., Shay, T.J., 1985. Intensive measurements

1059 of turbulence and shear in the equatorial undercurrent. *Nature* 318, 140–144.

1060 Groeskamp, S., Abernathey, R.P., Klocker, A., 2016. Water mass transformation by cabbeling

1061 and thermobaricity. *Geophysical Research Letters* 43, 2016GL070860.

1062 Groeskamp, S., Sloyan, B.M., Zika, J.D., McDougall, T.J., 2017. Mixing inferred from an

1063 ocean climatology and surface fluxes. *J. Phys. Oceanogr.* 47, 667–687.

1064 Groeskamp, S., Griffies, S.M., Iudicone, D., Marsh, R., Nurser, A.J.G., Zika, J.D., 2019. The

1065 water mass transformation framework for ocean physics and biogeochemistry. *Annual Re-*

1066 *view of Marine Science* 11, 271–305.

1067 Groeskamp, S., LaCasce, J.H., McDougall, T.J., Rogé, M., 2020. Full-depth global estimates of

1068 ocean mesoscale eddy mixing from observations and theory. *Geophysical Research Letters*

1069 47, e2020GL089425.

1070 Guilyardi, E., Madec, G., Terray, L., 2001. The role of lateral ocean physics in the upper ocean  
 1071 thermal balance of a coupled ocean-atmosphere GCM. *Climate Dynamics* 17, 589–599.  
 1072 Harrison, D.E., 1978. On the diffusion parameterization of mesoscale eddy effects from a  
 1073 numerical ocean experiment. *J. Phys. Oceanogr.* 8, 913–918.  
 1074 Hautala, S.L., Riser, S.C., 1993. A nonconservative  $\beta$ -spiral determination of the deep circula-  
 1075 tion in the eastern South Pacific. *J. Phys. Oceanogr.* 23, 1975–2000.  
 1076 Henning, C.C., Vallis, G.K., 2004. The effects of mesoscale eddies on the main subtropical  
 1077 thermocline. *J. Phys. Oceanogr.* 34, 2428–2443.  
 1078 Hieronymus, M., Nycander, J., 2013. The budgets of heat and salinity in NEMO. *Ocean Mod-*  
 1079 *elling* 67, 28–38.  
 1080 Hieronymus, M., Nycander, J., Nilsson, J., Döös, K., Hallberg, R., 2019. Oceanic overturning  
 1081 and heat transport: The role of background diffusivity. *J. Climate* 32, 701–716.  
 1082 Holland, W.R., 1978. The role of mesoscale eddies in the general circulation of the ocean—  
 1083 numerical experiments using a wind-driven quasi-geostrophic model. *J. Phys. Oceanogr.* 8,  
 1084 363–392.  
 1085 Holmes, R.M., de Lavergne, C., McDougall, T.J., 2018b. Ridges, seamounts, troughs, and  
 1086 bowls: Topographic control of the diapycnal circulation in the abyssal ocean. *J. Phys.*  
 1087 *Oceanogr.* 48, 861–882.  
 1088 Holmes, R.M., Zika, J.D., England, M.H., 2018a. Diathermal heat transport in a global ocean  
 1089 model. *J. Phys. Oceanogr.* 49, 141–161.  
 1090 Holmes, R.M., Zika, J.D., Ferrari, R., Thompson, A.F., Newsom, E.R., England, M.H., 2019.  
 1091 Atlantic ocean heat transport enabled by Indo-Pacific heat uptake and mixing. *Geophysical*  
 1092 *Research Letters* 46, 13939–13949.  
 1093 Holzer, M., Primeau, F.W., 2006. The diffusive ocean conveyor. *Geophysical Research Letters*  
 1094 33, L14618.

Howard, E., Hogg, A.McC., Waterman, S., Marshall, D.P., 2014. The injection of zonal momentum by buoyancy forcing in a Southern Ocean model. *J. Phys. Oceanogr.* 45, 259–271.

Huang, R.X., 1999. Mixing and energetics of the oceanic thermohaline circulation. *J. Phys. Oceanogr.* 29, 727–746.

Hughes, C.W., de Cuevas, B.A., 2001. Why western boundary currents in realistic oceans are inviscid: A link between form stress and bottom pressure torques. *J. Phys. Oceanogr.* 31, 2871–2885.

Hummels, R., Dengler, M., Boulès, B., 2013. Seasonal and regional variability of upper ocean diapycnal heat flux in the Atlantic cold tongue. *Progress in Oceanography* 111, 52–74.

Iselin, C.O., 1939. The influence of vertical and lateral turbulence on the characteristics of the waters at mid-depths. *Eos, Transactions American Geophysical Union* 20, 414–417.

Iudicone, D., Madec, G., Blanke, B., Speich, S., 2008. The role of Southern Ocean surface forcings and mixing in the global conveyor. *J. Phys. Oceanogr.* 38, 1377–1400.

Jackett, D.R., McDougall, T.J., 1997. A neutral density variable for the World’s Oceans. *J. Phys. Oceanogr.* 27, 237–263.

Jayne, S.R., 2009. The impact of abyssal mixing parameterizations in an ocean general circulation model. *J. Phys. Oceanogr.* 39, 1756–1775.

Jing, Z., Wu, L., 2014. Intensified diapycnal mixing in the midlatitude western boundary currents. *Sci. Rep.* 4.

Jochum, M., Briegleb, B.P., Danabasoglu, G., Large, W.G., Norton, N.J., Jayne, S.R., Alford, M.H., Bryan, F.O., 2012. The impact of oceanic near-inertial waves on climate. *J. Climate* 26, 2833–2844.

Johnson, G.C., Bryden, H.L., 1989. On the size of the Antarctic Circumpolar Current. *Deep Sea Research* 36, 39–53.

Jones, C.S., Abernathey, R.P., 2019. Isopycnal mixing controls deep ocean ventilation. *Geo-*

1120 physical Research Letters 46, 13144–13151.

1121 Klein, P., Treguier, A.-M., Hua, B.L., 1998. Three-dimensional stirring of thermohaline fronts.  
1122 Journal of Marine Research 56, 589–612.

1123 Klocker, A., Abernathey, R., 2014. Global patterns of mesoscale eddy properties and diffusivi-  
1124 ties. J. Phys. Oceanogr. 44, 1030–1046.

1125 Klocker, A., McDougall, T.J., 2010. Influence of the nonlinear equation of state on global  
1126 estimates of diapycnal advection and diffusion. J. Phys. Oceanogr. 40, 1690–1709.

1127 Koch-Larrouy, A., Lengaigne, M., Terray, P., Madec, G., Masson, S., 2010. Tidal mixing in  
1128 the Indonesian Seas and its effect on the tropical climate system. Climate Dynamics 34,  
1129 891–904.

1130 Kunze, E., Firing, E., Hummon, J.M., Chereskin, T.K., Thurnherr, A.M., 2006. Global abyssal  
1131 mixing inferred from lowered ADCP shear and CTD strain profiles. J. Phys. Oceanogr. 36,  
1132 1553–1576.

1133 Lagerloef, G.S.E., Mitchum, G.T., Lukas, R.B., Niiler, P.P., 1999. Tropical Pacific near-surface  
1134 currents estimated from altimeter, wind, and drifter data. J. Geophys. Res. 104, 23313–23326.

1135 Large, W.G., McWilliams, J.C., Doney, S.C., 1994. Oceanic vertical mixing: A review and a  
1136 model with a nonlocal boundary layer parameterization. Reviews of Geophysics 32, 363–403.

1137 Le Corre, M., Gula, J., Tréguier, A.-M., 2020. Barotropic vorticity balance of the North Atlantic  
1138 subpolar gyre in an eddy-resolving model. Ocean Science 16, 451–468.

1139 Ledwell, J.R., St Laurent, L.C., Girton, J.B., Toole, J.M., 2011. Diapycnal mixing in the Antarc-  
1140 tic Circumpolar Current. J. Phys. Oceanogr. 41, 241–246.

1141 Ledwell, J.R., Montgomery, E.T., Polzin, K.L., St Laurent, L.C., Schmitt, R.W., Toole, J.M.,  
1142 2000. Evidence for enhanced mixing over rough topography in the abyssal ocean. Nature  
1143 403, 179–182.

1144 Ledwell, J.R., Watson, A.J., Law, C.S., 1998. Mixing of a tracer in the pycnocline. J. Geophys.

1145 Res. 103, 21499–21529.

1146 Ledwell, J.R., Watson, A.J., Law, C.S., 1993. Evidence for slow mixing across the pycnocline  
1147 from an open-ocean tracer-release experiment. *Nature* 364, 701–703.

1148 Locarnini, R.A., Mishonov, A.V., Baranova, O.K., Boyer, T.P., Zweng, M.M., Garcia, H.E.,  
1149 Reagan, J.R., Seidov, D., Weathers, K., Paver, C.R., Smolyar, I., 2018. *World Ocean Atlas*  
1150 2018, Volume 1: Temperature. A. Mishonov Technical Ed.; NOAA Atlas NESDIS 81, 52 pp.

1151 Lozier, M.S., Li, F., Bacon, S., Bahr, F., Bower, A.S., Cunningham, S.A., Jong, M.F. de,  
1152 Steur, L. de, deYoung, B., Fischer, J., Gary, S.F., Greenan, B.J.W., Holliday, N.P., Houk,  
1153 A., Houpert, L., Inall, M.E., Johns, W.E., Johnson, H.L., Johnson, C., Karstensen, J., Koman,  
1154 G., Bras, I.A.L., Lin, X., Mackay, N., Marshall, D.P., Mercier, H., Olthmanns, M., Pickart,  
1155 R.S., Ramsey, A.L., Rayner, D., Straneo, F., Thierry, V., Torres, D.J., Williams, R.G., Wil-  
1156 son, C., Yang, J., Yashayaev, I., Zhao, J., 2019. A sea change in our view of overturning in  
1157 the subpolar North Atlantic. *Science* 363, 516–521.

1158 Lu, P., McCreary, J.P., Klinger, B.A., 1998. Meridional circulation cells and the source waters  
1159 of the Pacific equatorial undercurrent. *J. Phys. Oceanogr.* 28, 62–84.

1160 Lucazeau, F., 2019. Analysis and mapping of an updated terrestrial heat flow data set. *Geo-*  
1161 *chemistry, Geophysics, Geosystems* 20, 4001–4024.

1162 Lumpkin, R., Speer, K., 2007. Global ocean meridional overturning. *J. Phys. Oceanogr.* 37,  
1163 2550–2562.

1164 Lumpkin, R., Speer, K., 2003. Large-scale vertical and horizontal circulation in the North  
1165 Atlantic ocean. *J. Phys. Oceanogr.* 33, 1902–1920.

1166 Luyten, J.R., Pedlosky, J., Stommel, H., 1983. The ventilated thermocline. *J. Phys. Oceanogr.*  
1167 13, 292–309.

1168 MacKinnon, J.A., Johnston, T.M.S., Pinkel, R., 2008. Strong transport and mixing of deep  
1169 water through the Southwest Indian Ridge. *Nature Geoscience* 1, 755–758.

1170 Mantyla, A.W., Reid, J.L., 1983. Abyssal characteristics of the World Ocean waters. *Deep Sea*  
1171 *Research* 30, 805–833.

1172 Marshall, D., 1997. Subduction of water masses in an eddying ocean. *Journal of Marine Re-*  
1173 *search* 55, 201–222.

1174 Marshall, J.C., Nurser, A.J.G., 1991. A continuously stratified thermocline model incorporating  
1175 a mixed layer of variable thickness and density. *J. Phys. Oceanogr.* 21, 1780–1792.

1176 Marshall, J., Jones, H., Karsten, R., Wardle, R., 2002. Can eddies set ocean stratification? *J.*  
1177 *Phys. Oceanogr.* 32, 26–38.

1178 Marshall, J., Radko, T., 2003. Residual-mean solutions for the Antarctic Circumpolar Current  
1179 and its associated overturning circulation. *J. Phys. Oceanogr.* 33, 2341–2354.

1180 Marshall, J., Speer, K., 2012. Closure of the meridional overturning circulation through South-  
1181 ern Ocean upwelling. *Nature Geoscience* 5, 171–180.

1182 Mashayek, A., Ferrari, R., Merrifield, S., Ledwell, J.R., Laurent, L.S., Naveira Garabato, A.C.,  
1183 2017. Topographic enhancement of vertical turbulent mixing in the Southern Ocean. *Nature*  
1184 *Communications* 8, 14197.

1185 Mazloff, M.R., Ferrari, R., Schneider, T., 2013. The force balance of the Southern Ocean  
1186 meridional overturning circulation. *J. Phys. Oceanogr.* 43, 1193–1208.

1187 McCartney, M.S., 1977. Subantarctic Mode Water. In. *A Voyage of Discovery*, *Deep Sea*  
1188 *Research* 24, 103–119.

1189 McCreary, J.P., Lu, P., 1994. Interaction between the subtropical and equatorial ocean circula-  
1190 tions: The subtropical cell. *J. Phys. Oceanogr.* 24, 466–497.

1191 McDougall, T.J., 2003. Potential enthalpy: A conservative oceanic variable for evaluating heat  
1192 content and heat fluxes. *J. Phys. Oceanogr.* 33, 945–963.

1193 McDougall, T.J., 1984. The relative roles of diapycnal and isopycnal mixing on subsurface  
1194 water mass conversion. *J. Phys. Oceanogr.* 14, 1577–1589.

1195 McDougall, T.J., 1989. Dianeutral advection. *Parameterization of small-scale processes: Proc.*  
1196 *'Aha Huliko'a Hawaiian Winter Workshop*, Honolulu, HI, University of Hawaii at Manoa,  
1197 289-315.

1198 McDougall, T.J., Ferrari, R., 2017. Abyssal upwelling and downwelling driven by near-boundary  
1199 mixing. *J. Phys. Oceanogr.* 47, 261–283.

1200 McDougall, T.J., Groeskamp, S., Griffies, S.M., 2014. On geometrical aspects of interior ocean  
1201 mixing. *J. Phys. Oceanogr.* 44, 2164–2175.

1202 McDougall, T.J., Jackett, D.R., Millero, F.J., Pawlowicz, R., Barker, P.M., 2012. A global  
1203 algorithm for estimating Absolute Salinity. *Ocean Science* 8, 1123–1134.

1204 McDougall, T.J., McIntosh, P.C., 2001. The temporal-residual-mean velocity. Part II: Isopycnal  
1205 interpretation and the tracer and momentum equations. *J. Phys. Oceanogr.* 31, 1222–1246.

1206 McPhaden, M.J., Zhang, D., 2002. Slowdown of the meridional overturning circulation in the  
1207 upper Pacific Ocean. *Nature* 415, 603–608.

1208 McWilliams, J.C., Chow, J.H.S., 1981. Equilibrium geostrophic turbulence I: A reference solu-  
1209 tion in a  $\beta$ -plane channel. *J. Phys. Oceanogr.* 11, 921–949.

1210 Melet, A., Hallberg, R., Legg, S., Nikurashin, M., 2014. Sensitivity of the ocean state to lee  
1211 wave-driven mixing. *J. Phys. Oceanogr.* 44, 900–921.

1212 Melet, A., Legg, S., Hallberg, R., 2016. Climatic impacts of parameterized local and remote  
1213 tidal mixing. *J. Climate* 29, 3473–3500.

1214 Mercier, H., Speer, K.G., 1998. Transport of bottom water in the Romanche fracture zone and  
1215 the Chain fracture zone. *J. Phys. Oceanogr.* 28, 779–790.

1216 Meredith, M.P., Woodworth, P.L., Chereskin, T.K., Marshall, D.P., Allison, L.C., Bigg, G.R.,  
1217 Donohue, K., Heywood, K.J., Hughes, C.W., Hibbert, A., Hogg, A.M., Johnson, H.L., Jul-  
1218 lion, L., King, B.A., Leach, H., Lenn, Y.-D., Maqueda, M.A.M., Munday, D.R., Naveira  
1219 Garabato, A.C., Provost, C., Sallée, J.-B., Sprintall, J., 2011. Sustained monitoring of the



1220 Southern Ocean at Drake Passage: Past achievements and future priorities. *Reviews of Geo-*  
1221 *physics* 49.

1222 Moum, J.N., Lien, R.-C., Perlin, A., Nash, J.D., Gregg, M.C., Wiles, P.J., 2009. Sea surface  
1223 cooling at the Equator by subsurface mixing in tropical instability waves. *Nature Geoscience*  
1224 2, 761–765.

1225 Moum, J.N., Perlin, A., Nash, J.D., McPhaden, M.J., 2013. Seasonal sea surface cooling in the  
1226 equatorial Pacific cold tongue controlled by ocean mixing. *Nature* 500, 64–67.

1227 Munday, D.R., Allison, L.C., Johnson, H.L., Marshall, D.P., 2011. Remote forcing of the  
1228 Antarctic Circumpolar Current by diapycnal mixing. *Geophysical Research Letters* 38, L08609.

1229 Munk, W., 1997. Once again: once again—tidal friction. *Progress in Oceanography* 40, 7–35.

1230 Munk, W., Wunsch, C., 1998. Abyssal recipes II: Energetics of tidal and wind mixing. *Deep-*  
1231 *Sea Research* 45, 1977–2010.

1232 Munk, W.H., 1966. Abyssal recipes. *Deep Sea Research* 13, 707–730.

1233 Munk, W.H., 1950. On the wind-driven ocean circulation. *J. Meteor.* 7, 80–93.

1234 Munk, W.H., Palmén, E., 1951. Note on the dynamics of the Antarctic Circumpolar Current.  
1235 *Tellus* 3, 53–55.

1236 Naveira Garabato, A.C., Frajka-Williams, E., Spingys, C.P., Legg, S., Polzin, K.L., Forryan,  
1237 A., Abrahamsen, P., Buckingham, C., Griffies, S.M., McPhail, S., Nicholls, K., Thomas,  
1238 L.N., Meredith, M., 2019. Rapid mixing and exchange of deep-ocean waters in an abyssal  
1239 boundary current. *Proceedings of the National Academy of Sciences* 116, 13233–13238.

1240 Naveira Garabato, A.C., MacGilchrist, G.A., Brown, P.J., Evans, D.G., Meijers, A.J.S., Zika,  
1241 J.D., 2017. High-latitude ocean ventilation and its role in Earth’s climate transitions. *Phil.*  
1242 *Trans. R. Soc. A* 375, 20160324.

1243 Naveira Garabato, A.C., Polzin, K.L., Ferrari, R., Zika, J.D., Forryan, A., 2016. A microscale  
1244 view of mixing and overturning across the Antarctic Circumpolar Current. *J. Phys. Oceanogr.*

1245 46, 233–254.

1246 Naveira Garabato, A.C., Stevens, D.P., Watson, A.J., Roether, W., 2007. Short-circuiting of the  
 1247 overturning circulation in the Antarctic Circumpolar Current. *Nature* 447, 194–197.

1248 Naveira Garabato, A.C., Williams, A.P., Bacon, S., 2014. The three-dimensional overturning  
 1249 circulation of the Southern Ocean during the WOCE era. *Progress in Oceanography* 120,  
 1250 41–78.

1251 Nikurashin, M., Vallis, G., 2012. A theory of the interhemispheric meridional overturning  
 1252 circulation and associated stratification. *J. Phys. Oceanogr.* 42, 1652–1667.

1253 Nurser, A.J.G., Marsh, R., Williams, R.G., 1999. Diagnosing water mass formation from air-sea  
 1254 fluxes and surface mixing. *J. Phys. Oceanogr.* 29, 1468–1487.

1255 Nycander, J., Hieronymus, M., Roquet, F., 2015. The nonlinear equation of state of sea water  
 1256 and the global water mass distribution. *Geophysical Research Letters* 42, 2015GL065525.

1257 Nycander, J., Nilsson, J., Döös, K., Broström, G., 2007. Thermodynamic analysis of ocean  
 1258 circulation. *J. Phys. Oceanogr.* 37, 2038–2052.

1259 Oakey, N.S., 1982. Determination of the rate of dissipation of turbulent energy from simultane-  
 1260 ous temperature and velocity shear microstructure measurements. *J. Phys. Oceanogr.* 12,  
 1261 256–271.

1262 Olbers, D., 1998. Comments on “On the obscurantist physics of ‘Form Drag’ in theorizing  
 1263 about the Circumpolar Current.” *J. Phys. Oceanogr.* 28, 1647–1654.

1264 Orsi, A.H., Johnson, G.C., Bullister, J.L., 1999. Circulation, mixing, and production of Antarc-  
 1265 tic Bottom Water. *Progress in Oceanography* 43, 55–109.

1266 Osborn, T.R., 1978. Measurements of energy dissipation adjacent to an island. *J. Geophys.*  
 1267 *Res.* 83, 2939.

1268 Osborn, T.R., Cox, C.S., 1972. Oceanic fine structure. *Geophysical Fluid Dynamics* 3, 321–345.

1269 Pacanowski, R.C., 1987. Effect of equatorial currents on surface stress. *J. Phys. Oceanogr.* 17,

1270 833–838.

1271 Pedlosky, J., 1996. Ocean circulation theory. Springer, Berlin, 453 pp.

1272 Pedlosky, J., 1992. The baroclinic structure of the abyssal circulation. *J. Phys. Oceanogr.* 22,  
1273 652–659.

1274 Pellichero, V., Sallée, J.-B., Schmidtko, S., Roquet, F., Charrassin, J.-B., 2017. The ocean  
1275 mixed layer under Southern Ocean sea-ice: Seasonal cycle and forcing. *J. Geophys. Res.*  
1276 122, 1608–1633.

1277 PeñaMolino, B., Rintoul, S.R., Mazloff, M.R., 2014. Barotropic and baroclinic contributions to  
1278 along-stream and across-stream transport in the Antarctic Circumpolar Current. *J. Geophys.*  
1279 *Res.* 119, 8011–8028.

1280 Pickart, R.S., Spall, M.A., 2007. Impact of Labrador Sea convection on the North Atlantic  
1281 meridional overturning circulation. *J. Phys. Oceanogr.* 37, 2207–2227.

1282 Plant, W.J., 1982. A relationship between wind stress and wave slope. *J. Geophys. Res.* 87,  
1283 1961–1967.

1284 Pollard, R.T., Rhines, P.B., Thompson, R.O., 1973. The deepening of the wind-mixed layer.  
1285 *Geophys. Astrophys. Fluid Dyn.* 4, 381–404.

1286 Polzin, K.L., Speer, K.G., Toole, J.M., Schmitt, R.W., 1996. Intense mixing of Antarctic Bottom  
1287 Water in the equatorial Atlantic Ocean. *Nature* 380, 54–57.

1288 Polzin, K.L., Toole, J.M., Ledwell, J.R., Schmitt, R.W., 1997. Spatial variability of turbulent  
1289 mixing in the abyssal ocean. *Science* 276, 93–96.

1290 Price, J.F., Weller, R.A., Pinkel, R., 1986. Diurnal cycling: Observations and models of the  
1291 upper ocean response to diurnal heating, cooling, and wind mixing. *J. Geophys. Res.* 91,  
1292 8411–8427.

1293 Price, J.F., 2001. Chapter 5.3 - Subduction, in: Siedler, G., Church, J., Gould, J. (Eds.), *Inter-*  
1294 *national Geophysics, Ocean Circulation and Climate.* Academic Press, pp. 357–371.

1295 Pujol, M.-I., Faugère, Y., Taburet, G., Dupuy, S., Pelloquin, C., Ablain, M., Picot, N., 2016.  
1296 DUACS DT2014: the new multi-mission altimeter data set reprocessed over 20 years. *Ocean*  
1297 *Science* 12, 1067–1090.

1298 Qu, T., Gao, S., Fine, R.A., 2013. Subduction of South Pacific tropical water and its equator-  
1299 ward pathways as shown by a simulated passive tracer. *J. Phys. Oceanogr.* 43, 1551-1565.

1300 Ragen, S., Pradal, M.-A., Gnanadesikan, A., 2020. The impact of parameterized lateral mixing  
1301 on the Antarctic Circumpolar Current in a coupled climate model. *J. Phys. Oceanogr.* 50,  
1302 965–982.

1303 Reid, J.L., 2003. On the total geostrophic circulation of the Indian ocean: flow patterns, tracers,  
1304 and transports. *Progress in Oceanography* 56, 137–186.

1305 Reid, J.L., 1997. On the total geostrophic circulation of the Pacific ocean: flow patterns, tracers,  
1306 and transports. *Progress in Oceanography* 39, 263–352.

1307 Rhines, P.B., 1993. Oceanic General Circulation: Wave and Advection Dynamics, in: Wille-  
1308 brand, J., Anderson, D.L.T. (Eds.), *Modelling Oceanic Climate Interactions*, NATO ASI Se-  
1309 ries. Springer, Berlin, Heidelberg, pp. 67–149.

1310 Rhines, P.B., Holland, W.R., 1979. A theoretical discussion of eddy-driven mean flows. *Dy-*  
1311 *namics of Atmospheres and Oceans* 3, 289–325.

1312 Rhines, P.B., Young, W.R., 1982. Homogenization of potential vorticity in planetary gyres.  
1313 *Journal of Fluid Mechanics* 122, 347–367.

1314 Rintoul, S.R., Naveira Garabato, A.C., 2013. Chapter 18 - Dynamics of the Southern Ocean  
1315 Circulation, in: Siedler, G., Griffies, S.M., Gould, J., Church, J.A. (Eds.), *International Geo-*  
1316 *physics, Ocean Circulation and Climate*. Academic Press, pp. 471–492.

1317 Robbins, P.E., Price, J.F., Owens, W.B., Jenkins, W.J., 2000. The importance of lateral diffu-  
1318 sion for the ventilation of the lower thermocline in the subtropical North Atlantic. *J. Phys.*  
1319 *Oceanogr.* 30, 67–89.

1320 Roemmich, D., 1983. The balance of geostrophic and Ekman transports in the tropical Atlantic  
 1321 Ocean. *J. Phys. Oceanogr.* 13, 1534–1539.

1322 Roquet, F., Wunsch, C., Madec, G., 2011. On the patterns of wind-power input to the ocean  
 1323 circulation. *J. Phys. Oceanogr.* 41, 2328–2342.

1324 Rudnick, D.L., Boyd, T.J., Brainard, R.E., Carter, G.S., Egbert, G.D., Gregg, M.C., Holloway,  
 1325 P.E., Klymak, J.M., Kunze, E., Lee, C.M., Levine, M.D., Luther, D.S., Martin, J.P., Merri-  
 1326 field, M.A., Moum, J.N., Nash, J.D., Pinkel, R., Rainville, L., Sanford, T.B., 2003. From  
 1327 tides to mixing along the Hawaiian ridge. *Science* 301, 355–357.

1328 Samelson, R.M., Vallis, G.K., 1997. Large-scale circulation with small diapycnal diffusion:  
 1329 The two-thermocline limit. *Journal of Marine Research* 55, 223–275.

1330 Sarmiento, J.L., Simeon, J., Gnanadesikan, A., Gruber, N., Key, R.M., Schlitzer, R., 2007.  
 1331 Deep ocean biogeochemistry of silicic acid and nitrate. *Global Biogeochemical Cycles* 21,  
 1332 GB1S90.

1333 Sasaki, H., Kida, S., Furue, R., Nonaka, M., Masumoto, Y., 2018. An increase of the Indone-  
 1334 sian Throughflow by internal tidal mixing in a high-resolution quasi-global ocean simulation.  
 1335 *Geophysical Research Letters* 45, 8416–8424.

1336 Schmitz, W.J., 1995. On the interbasin-scale thermohaline circulation. *Rev. Geophys.* 33,  
 1337 151–173.

1338 Schmitz, W.J., Richardson, P.L., 1991. On the sources of the Florida Current. *Deep-Sea Res.*  
 1339 38, S379–S409.

1340 Sheen, K.L., Brearley, J.A., Naveira Garabato, A.C., Smeed, D.A., Waterman, S., Ledwell, J.R.,  
 1341 Meredith, M.P., St. Laurent, L., Thurnherr, A.M., Toole, J.M., Watson, A.J., 2013. Rates and  
 1342 mechanisms of turbulent dissipation and mixing in the Southern Ocean: Results from the  
 1343 Diapycnal and Isopycnal Mixing Experiment in the Southern Ocean (DIMES). *J. Geophys.*  
 1344 *Res.* 118, 2774–2792.

- 1345 Sloyan, B.M., Johnson, G.C., Kessler, W.S., 2003. The Pacific cold tongue: A pathway for  
1346 interhemispheric exchange. *J. Phys. Oceanogr.* 33, 1027–1043.
- 1347 Sloyan, B.M., Rintoul, S.R., 2001. The Southern Ocean limb of the global deep overturning  
1348 circulation. *J. Phys. Oceanogr.* 31, 143–173.
- 1349 Sloyan, B.M., Talley, L.D., Chereskin, T.K., Fine, R., Holte, J., 2010. Antarctic Intermediate  
1350 Water and Subantarctic Mode Water formation in the southeast Pacific: The role of turbulent  
1351 mixing. *J. Phys. Oceanogr.* 40, 1558–1574.
- 1352 Smith, K.S., Ferrari, R., 2009. The production and dissipation of compensated thermohaline  
1353 variance by mesoscale stirring. *J. Phys. Oceanogr.* 39, 2477–2501.
- 1354 Smith, R.D., McWilliams, J.C., 2003. Anisotropic horizontal viscosity for ocean models. *Ocean*  
1355 *Modelling* 5, 129–156.
- 1356 Smyth, W.D., Moum, J.N., 2013. Marginal instability and deep cycle turbulence in the eastern  
1357 equatorial Pacific Ocean. *Geophysical Research Letters* 40, 6181–6185.
- 1358 St. Laurent, L., Naveira Garabato, A.C., Ledwell, J.R., Thurnherr, A.M., Toole, J.M., Watson,  
1359 A.J., 2012. Turbulence and diapycnal mixing in Drake Passage. *J. Phys. Oceanogr.* 42,  
1360 2143–2152.
- 1361 St. Laurent, L.C., Toole, J.M., Schmitt, R.W., 2001. Buoyancy forcing by turbulence above  
1362 rough topography in the abyssal Brazil Basin. *J. Phys. Oceanogr.* 31, 3476–3495.
- 1363 Stewart, A.L., Hogg, A.McC., 2017. Reshaping the Antarctic Circumpolar Current via Antarc-  
1364 tic Bottom Water export. *J. Phys. Oceanogr.* 47, 2577–2601.
- 1365 Stommel, H., 1979. Determination of water mass properties of water pumped down from the  
1366 Ekman layer to the geostrophic flow below. *Proceedings of National Academy of Sciences*  
1367 76, 3051–3055.
- 1368 Stommel, H., 1958. The abyssal circulation. *Deep Sea Research* 5, 80–82.
- 1369 Stommel, H., Arons, A.B., 1959a. On the abyssal circulation of the world ocean—II. An ideal-

1370     ized model of the circulation pattern and amplitude in oceanic basins. *Deep Sea Research* 6,  
1371     217–233.

1372     Stommel, H., Arons, A.B., 1959b. On the abyssal circulation of the world ocean—I. Stationary  
1373     planetary flow patterns on a sphere. *Deep Sea Research* 6, 140–154.

1374     Su, Z., Stewart, A.L., Thompson, A.F., 2014. An idealized model of Weddell Gyre export  
1375     variability. *J. Phys. Oceanogr.* 44, 1671–1688.

1376     Sun, S., Eisenman, I., Zanna, L., Stewart, A.L., 2020. Surface constraints on the depth of  
1377     the Atlantic meridional overturning circulation: Southern Ocean versus North Atlantic. *J.*  
1378     *Climate* 33, 3125–3149.

1379     Sweeney, C., Gnanadesikan, A., Griffies, S.M., Harrison, M.J., Rosati, A.J., Samuels, B.L.,  
1380     2005. Impacts of shortwave penetration depth on large-scale ocean circulation and heat trans-  
1381     port. *J. Phys. Oceanogr.* 35, 1103–1119.

1382     Taburet, G., Sanchez-Roman, A., Ballarotta, M., Pujol, M.-I., Legeais, J.-F., Fournier, F.,  
1383     Faugere, Y., Dibarboure, G., 2019. DUACS DT2018: 25 years of reprocessed sea level  
1384     altimetry products. *Ocean Science* 15, 1207–1224.

1385     Talley, L., 2013. Closure of the global overturning circulation through the Indian, Pacific, and  
1386     Southern Oceans: Schematics and transports. *Oceanography* 26, 80–97.

1387     Tamsitt, V., Abernathey, R.P., Mazloff, M.R., Wang, J., Talley, L.D., 2018. Transformation of  
1388     deep water masses along Lagrangian upwelling pathways in the Southern Ocean. *J. Geophys.*  
1389     *Res.* 123, 1994–2017.

1390     Tamsitt, V., Drake, H.F., Morrison, A.K., Talley, L.D., Dufour, C.O., Gray, A.R., Griffies, S.M.,  
1391     Mazloff, M.R., Sarmiento, J.L., Wang, J., Weijer, W., 2017. Spiraling pathways of global  
1392     deep waters to the surface of the Southern Ocean. *Nature Communications* 8, 172.

1393     Thompson, A.F., Stewart, A.L., Spence, P., Heywood, K.J., 2018. The Antarctic slope current  
1394     in a changing climate. *Reviews of Geophysics* 56, 741–770.

- 1395 Toggweiler, J.R., Druffel, E.R.M., Key, R.M., Galbraith, E.D., 2019a. Upwelling in the ocean  
1396 basins north of the ACC: 1. On the upwelling exposed by the surface distribution of  $\Delta^{14}\text{C}$ . J.  
1397 Geophys. Res. 124, 2591–2608.
- 1398 Toggweiler, J.R., Druffel, E.R.M., Key, R.M., Galbraith, E.D., 2019b. Upwelling in the ocean  
1399 basins north of the ACC: 2. How cool subantarctic water reaches the surface in the tropics. J.  
1400 Geophys. Res. 124, 2609–2625.
- 1401 Toggweiler, J.R., Samuels, B., 1998. On the ocean’s large-scale circulation near the limit of no  
1402 vertical mixing. J. Phys. Oceanogr. 28, 1832–1852.
- 1403 Toggweiler, J.R., Samuels, B., 1995. Effect of Drake Passage on the global thermohaline circu-  
1404 lation. Deep Sea Research 42, 477–500.
- 1405 Toggweiler, J.R., Samuels, B., 1993. New Radiocarbon Constraints on the Upwelling of Abyssal  
1406 Water to the Ocean’s Surface, in: Heimann, M. (Ed.), The Global Carbon Cycle, NATO ASI  
1407 Series. Springer Berlin Heidelberg, pp. 333–366.
- 1408 Toole, J.M., Schmitt, R.W., Polzin, K.L., 1994. Estimates of diapycnal mixing in the abyssal  
1409 ocean. Science 264, 1120–1123.
- 1410 Treguier, A.M., Held, I.M., Larichev, V.D., 1997. Parameterization of quasigeostrophic eddies  
1411 in primitive equation ocean models. J. Phys. Oceanogr. 27, 567–580.
- 1412 Urakawa, L.S., Hasumi, H., 2012. Eddy-resolving model estimate of the cabbeling effect on  
1413 the water mass transformation in the Southern Ocean. J. Phys. Oceanogr. 42, 1288–1302.
- 1414 van Haren, H., Gostiaux, L., 2012. Detailed internal wave mixing above a deep-ocean slope.  
1415 Journal of Marine Research 70, 173–197.
- 1416 Vic, C., Naveira Garabato, A.C., Green, J.A.M., Waterhouse, A.F., Zhao, Z., Melet, A., Lavergne,  
1417 C. de, Buijsman, M.C., Stephenson, G.R., 2019. Deep-ocean mixing driven by small-scale  
1418 internal tides. Nature Communications 10, 2099.
- 1419 Voet, G., Girton, J.B., Alford, M.H., Carter, G.S., Klymak, J.M., Mickett, J.B., 2014. Pathways,



1420 volume transport, and mixing of abyssal water in the Samoan Passage. *J. Phys. Oceanogr.*  
 1421 45, 562–588.

1422 Walin, G., 1982. On the relation between sea-surface heat flow and thermal circulation in the  
 1423 ocean. *Tellus* 34, 187–195.

1424 Walin, G., 1977. A theoretical framework for the description of estuaries. *Tellus* 29, 128–136.

1425 Wang, Z., Meredith, M.P., 2008. Density-driven southern hemisphere subpolar gyres in coupled  
 1426 climate models. *Geophysical Research Letters* 35, L14608.

1427 Waterhouse, A.F., MacKinnon, J.A., Nash, J.D., Alford, M.H., Kunze, E., Simmons, H.L.,  
 1428 Polzin, K.L., St. Laurent, L.C., Sun, O.M., Pinkel, R., Talley, L.D., Whalen, C.B., Huussen,  
 1429 T.N., Carter, G.S., Fer, I., Waterman, S., Naveira Garabato, A.C., Sanford, T.B., Lee, C.M.,  
 1430 2014. Global patterns of diapycnal mixing from measurements of the turbulent dissipation  
 1431 rate. *J. Phys. Oceanogr.* 44, 1854–1872.

1432 Watson, A.J., Ledwell, J.R., Messias, M.-J., King, B.A., Mackay, N., Meredith, M.P., Mills, B.,  
 1433 Naveira Garabato, A.C., 2013. Rapid cross-density ocean mixing at mid-depths in the Drake  
 1434 Passage measured by tracer release. *Nature* 501, 408–411.

1435 Whalen, C.B., MacKinnon, J.A., Talley, L.D., 2018. Large-scale impacts of the mesoscale  
 1436 environment on mixing from wind-driven internal waves. *Nature Geoscience* 11, 842.

1437 Wolfe, C.L., Cessi, P., 2011. The adiabatic pole-to-pole overturning circulation. *J. Phys.*  
 1438 *Oceanogr.* 41, 1795–1810.

1439 Wunsch, C., 1997. The vertical partition of oceanic horizontal kinetic energy. *J. Phys. Oceanogr.*  
 1440 27, 1770–1794.

1441 Wunsch, C., 1970. On oceanic boundary mixing. *Deep Sea Research* 17, 293–301.

1442 Wunsch, C., Ferrari, R., 2004. Vertical mixing, energy, and the general circulation of the  
 1443 oceans. *Annual Review of Fluid Mechanics* 36, 281–314.

1444 Yang, X., Tziperman, E., Speer, K., 2020. Dynamics of deep ocean eastern boundary currents.

1445 Geophysical Research Letters 47, e2019GL085396.

1446 Zhai, X., Greatbatch, R.J., Eden, C., Hibiya, T., 2009. On the loss of wind-induced near-inertial  
 1447 energy to turbulent mixing in the upper ocean. *J. Phys. Oceanogr.* 39, 3040–3045.

1448 Zhai, X., Johnson, H.L., Marshall, D.P., 2010. Significant sink of ocean-eddy energy near  
 1449 western boundaries. *Nature Geoscience* 3, 608–612.

1450 Zhang, R., Delworth, T.L., Rosati, A., Anderson, W.G., Dixon, K.W., Lee, H.-C., Zeng, F.,  
 1451 2011. Sensitivity of the North Atlantic ocean circulation to an abrupt change in the Nordic  
 1452 Sea overflow in a high resolution global coupled climate model. *J. Geophys. Res.* 116,  
 1453 C12024.

1454 Zhu, Y., Zhang, R.-H., 2019. A modified vertical mixing parameterization for its improved  
 1455 ocean and coupled simulations in the tropical Pacific. *J. Phys. Oceanogr.* 49, 21–37.

1456 Zika, J.D., Le Sommer, J., Dufour, C.O., Molines, J.-M., Barnier, B., Brasseur, P., Dussin, R.,  
 1457 Penduff, T., Iudicone, D., Lenton, A., Madec, G., Mathiot, P., Orr, J., Shuckburgh, E., Vivier,  
 1458 F., 2012. Vertical eddy fluxes in the Southern Ocean. *J. Phys. Oceanogr.* 43, 941–955.

1459 Zika, J.D., Skliris, N., Nurser, A.J.G., Josey, S.A., Mudryk, L., Laliberté, F., Marsh, R., 2015.  
 1460 Maintenance and broadening of the ocean’s salinity distribution by the water cycle. *J. Climate*  
 1461 28, 9550–9560.

1462 Zika, J.D., Sloyan, B.M., McDougall, T.J., 2009. Diagnosing the Southern Ocean overturning  
 1463 from tracer fields. *J. Phys. Oceanogr.* 39, 2926–2940.

1464 Zweng, M. M., Reagan, J.R., Seidov, D., Boyer, T.P., Locarnini, R.A., Garcia, H.E., Mishonov,  
 1465 A.V., Baranova, O.K., Weathers, K., Paver, C.R., Smolyar, I., 2018. World Ocean Atlas 2018,  
 1466 Volume 2: Salinity. A. Mishonov Technical Ed.; NOAA Atlas NESDIS 82, 50 pp.

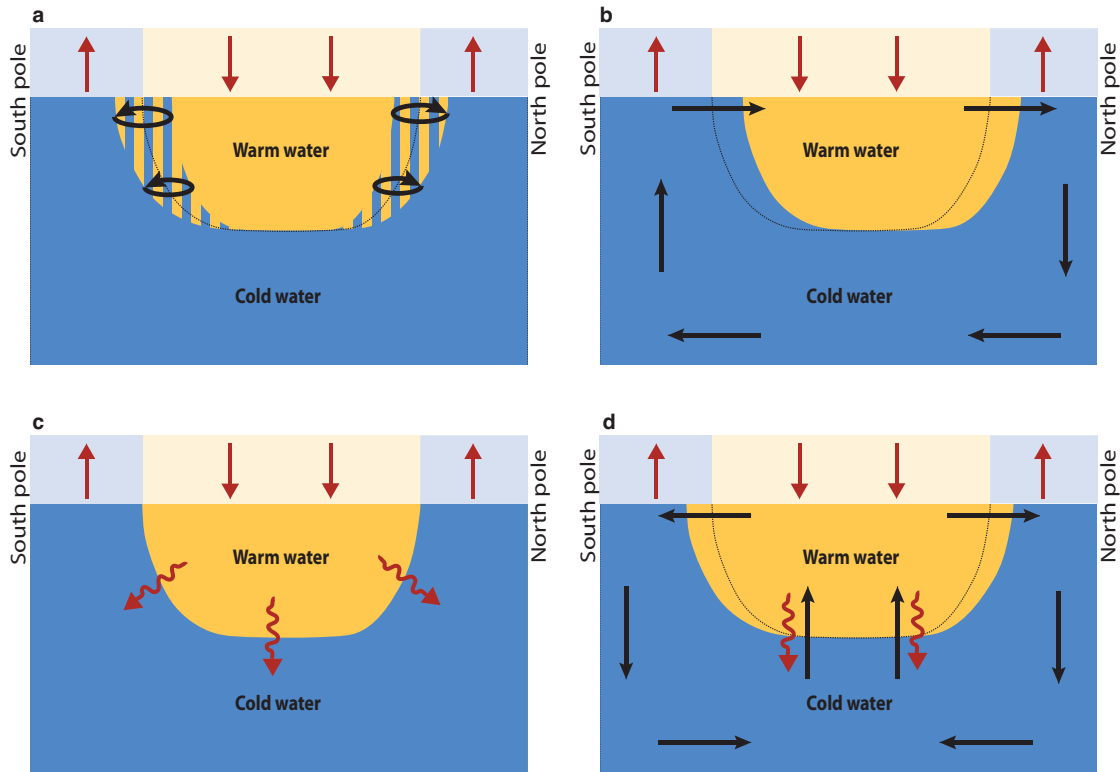


**Figure 1:** Idealised two-layer ocean composed of a warm bowl overlying a cold pool. Heating and cooling at the surface occurs within fixed latitudinal bands, represented by light blue (cooling) and light yellow (heating) colors. Salinity and freshwater fluxes are ignored. Straight and wiggly red arrows represent surface and interior heat fluxes, respectively. Black arrows represent mass transports. Each panel corresponds to a distinct scenario of poleward oceanic heat transport. Shown variations in the position and shape of the warm bowl are illustrative and partly arbitrary. **a**, Horizontal circulation moves warm water into the cooling latitudes and cold water into the warming latitudes. **b**, An inter-hemispheric overturning circulation shifts the warm bowl northward, reducing net heat gain (loss) of warm (cold) waters. **c**, Mixing transfers heat from the warm bowl to the cold pool. Note that we implicitly assume that mixing within each layer maintains temperature homogeneity, and thus connects surface and interior heat fluxes. **d**, Mixing converts cold waters into warm waters, allowing hemispheric overturning circulations to develop and transport heat poleward. Part of the diffusive heat gain of the lower layer may also offset surface cooling via intra-layer heat transports, as in **c**.

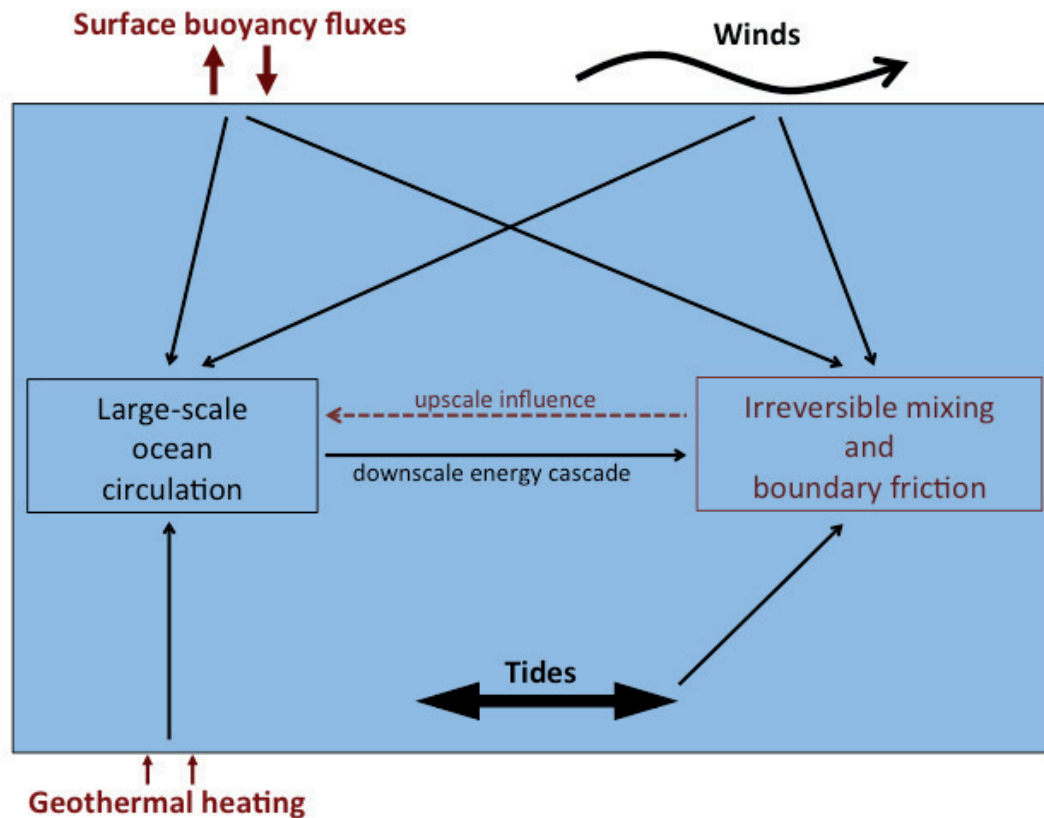


**Figure 2:** Simplified schematic of energy flows in the ocean, from forcing to dissipation. Forcing boils down to surface buoyancy fluxes, surface winds, tides (caused by gravitational interaction with the Moon and Sun), and geothermal heating along the seafloor. The large-scale ocean circulation is forced directly by large-scale wind and buoyancy forcing, and indirectly by irreversible mixing. Energy of the large-scale circulation is ultimately dissipated by boundary friction (drag) and irreversible mixing. Irreversible mixing includes momentum, temperature and salinity mixing at molecular scale. Mixing is energized directly by tides, winds, surface buoyancy fluxes and indirectly by the energy cascade from large-scale circulation to turbulence. Note that energy fuelling irreversible mixing and boundary friction is either lost as heat (momentum mixing and drag) or does work against gravity (mixing-driven buoyancy fluxes). The direct forcing of global ocean circulation by tides is thought to be secondary (Bessi res et al. 2008) and is therefore not highlighted here, despite known contributions to regional circulation features (e.g., Thompson et al. 2018, Chapter 2).

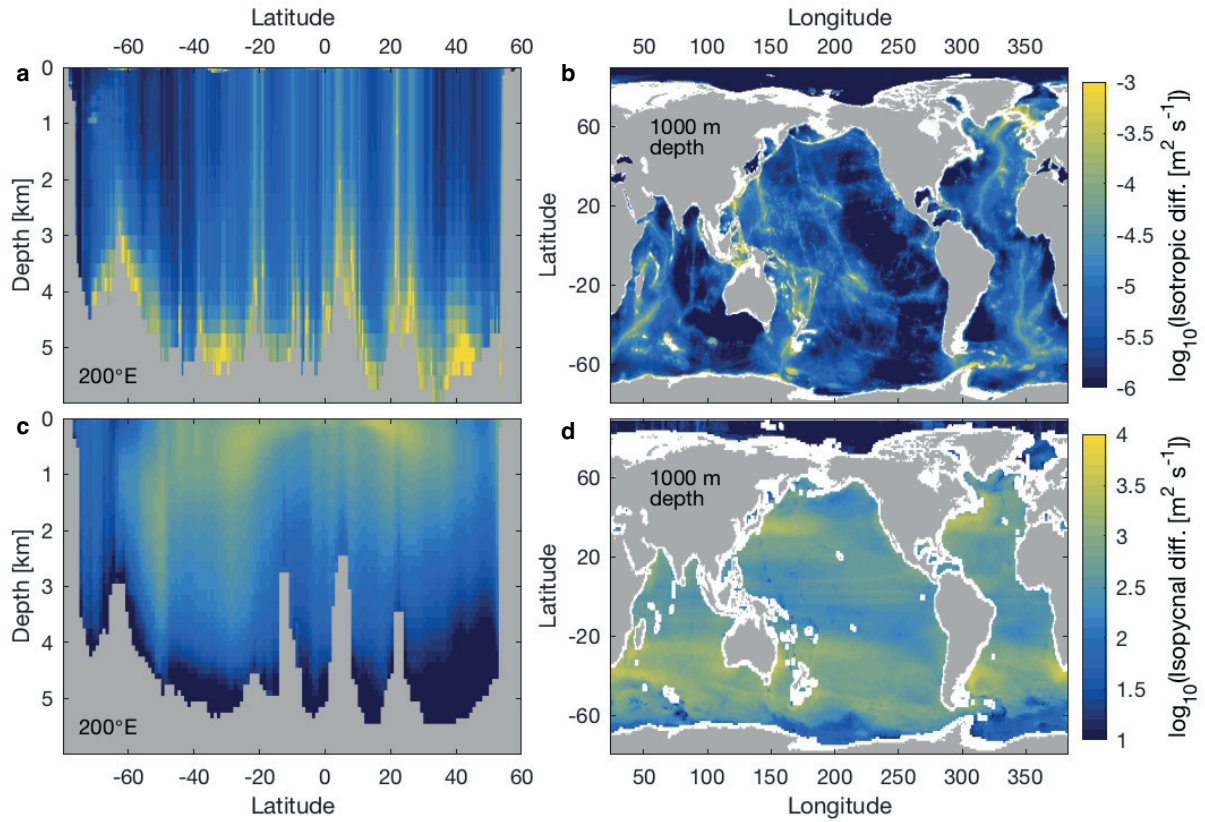


**Figure 3:** Estimated isotropic (a,b) and isopycnal (c,d) diffusivities, at 200°E/160°W (a,c) and at 1000 m depth (b,d). Both diffusivities are shown on a  $\log_{10}$  scale that spans three orders of magnitude (see colorscales on the right). Isotropic diffusivity here only includes the contribution of internal waves energized by tides (de Lavergne et al. 2020). Isopycnal diffusivity quantifies rates of mesoscale stirring (Groeskamp et al. 2020).

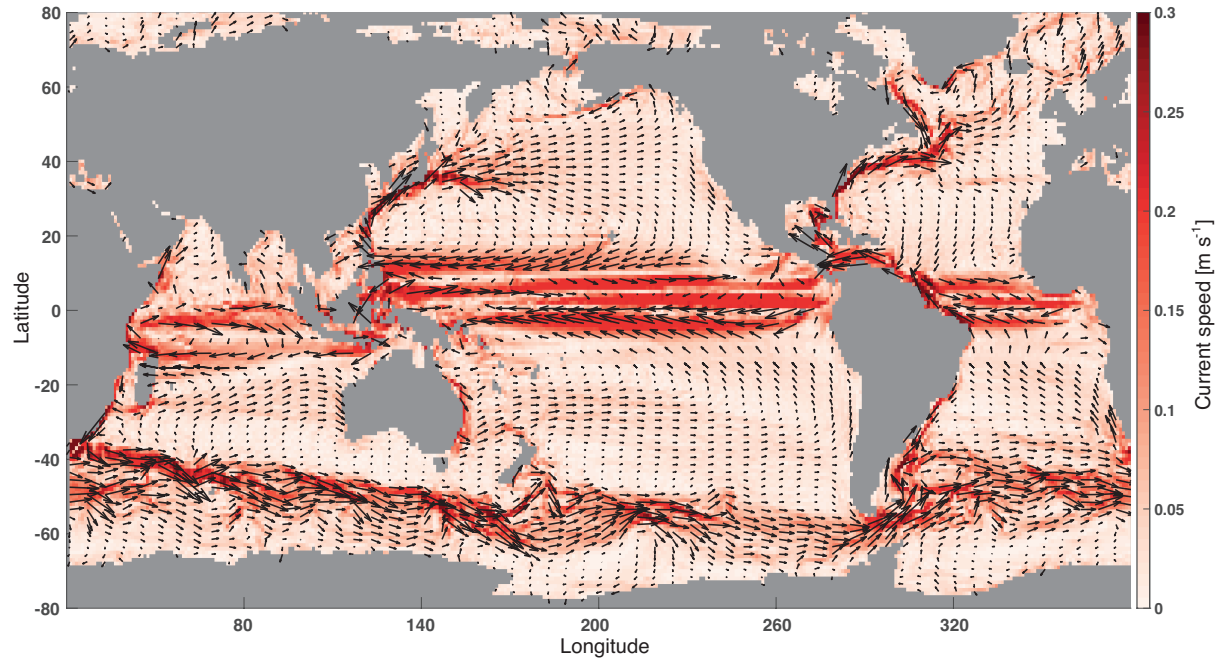


**Figure 4:** Annual mean surface geostrophic currents calculated using satellite observations. Surface geostrophic velocity obtained from the CMEMS (Copernicus Marine Environment Monitoring Service) operational delayed-time sea surface geostrophic velocity anomalies derived from satellite altimetry (Pujol et al. 2016, Taburet et al. 2019), using a  $\beta$ -plane approximation of the geostrophic equations in the equatorial band (Lagerhoef et al. 1999). Daily, quarter degree resolution data since 1993 is averaged and smoothed into a mean for illustrative purposes. Color is indicative of the speed, with darker colors being faster currents.

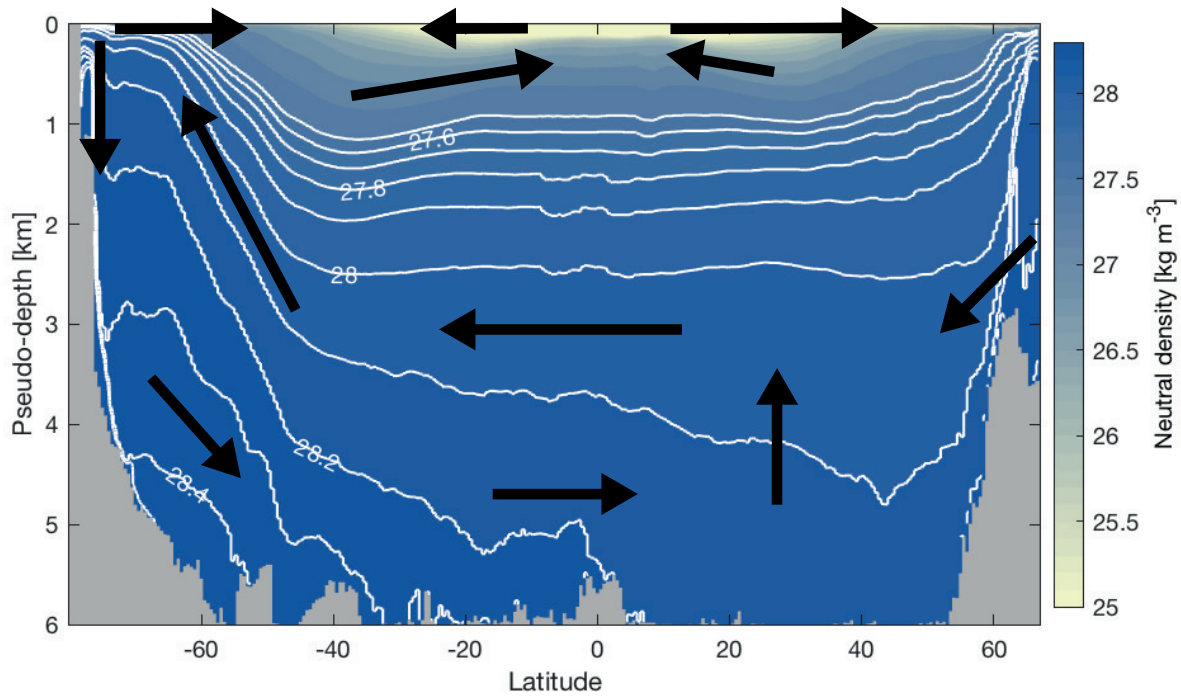


**Figure 5:** Global neutral density stratification and schematic meridional overturning circulation. The shading shows neutral density (Jackett and McDougall 1997) mapped by Gouretski and Koltermann (2004) as a function of latitude and pseudo-depth. The pseudo-depth of density surfaces is found by filling each latitude band from the bottom up with ocean grid cells ordered from dense to light. The neutral density range  $27.5\text{--}28.5 \text{ kg m}^{-3}$  is contoured in white with a  $0.1 \text{ kg m}^{-3}$  interval. Black arrows give a simplified view of overturning flows.

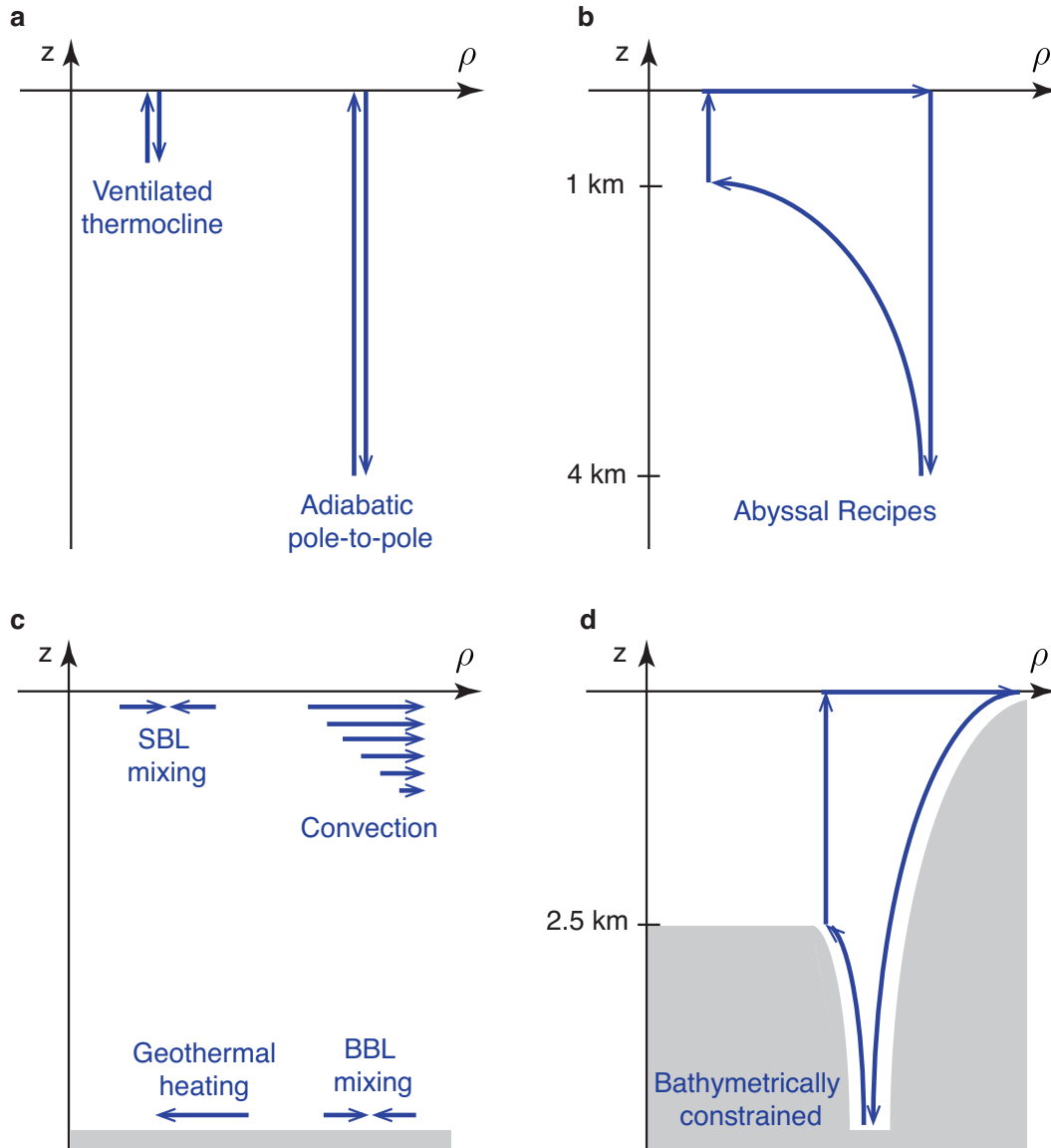


**Figure 6:** Idealized circulations viewed in density-depth coordinates. **a**, The ventilated thermocline (Luyten et al. 1983) and adiabatic pole-to-pole (Toggweiler and Samuels 1998, Wolfe and Cessi 2011) circulation frameworks involve flow along isopycnals only (with density transformations, i.e. movement along the  $x$ -axis, allowed only at the surface). **b**, The overturning circulation as modelled in the Abyssal Recipes of Munk and Wunsch (1998): dense waters sink at high latitudes down to 4 km depth and return to 1 km depth via mixing-driven upwelling across the low-latitude stratification. **c**, Schematic view of water parcel movements associated with mixing in the surface boundary layer (SBL), convective mixing forced by surface buoyancy loss, mixing in the bottom boundary layer (BBL), and geothermal heating. **d**, Proposed view of the overturning circulation: dense waters sink along the ocean floor, losing a large fraction of their density excess as they descend to abyssal depths and mix with overlying waters; mixing near the bottom and geothermal heating allows them to return to lighter layers up to 2.5 km depth; adiabatic Southern Ocean upwelling brings them from 2.5 km depth to the surface. The gray shading emphasizes the role of bathymetric constraints but does not imply that flow is disallowed within this phase space.



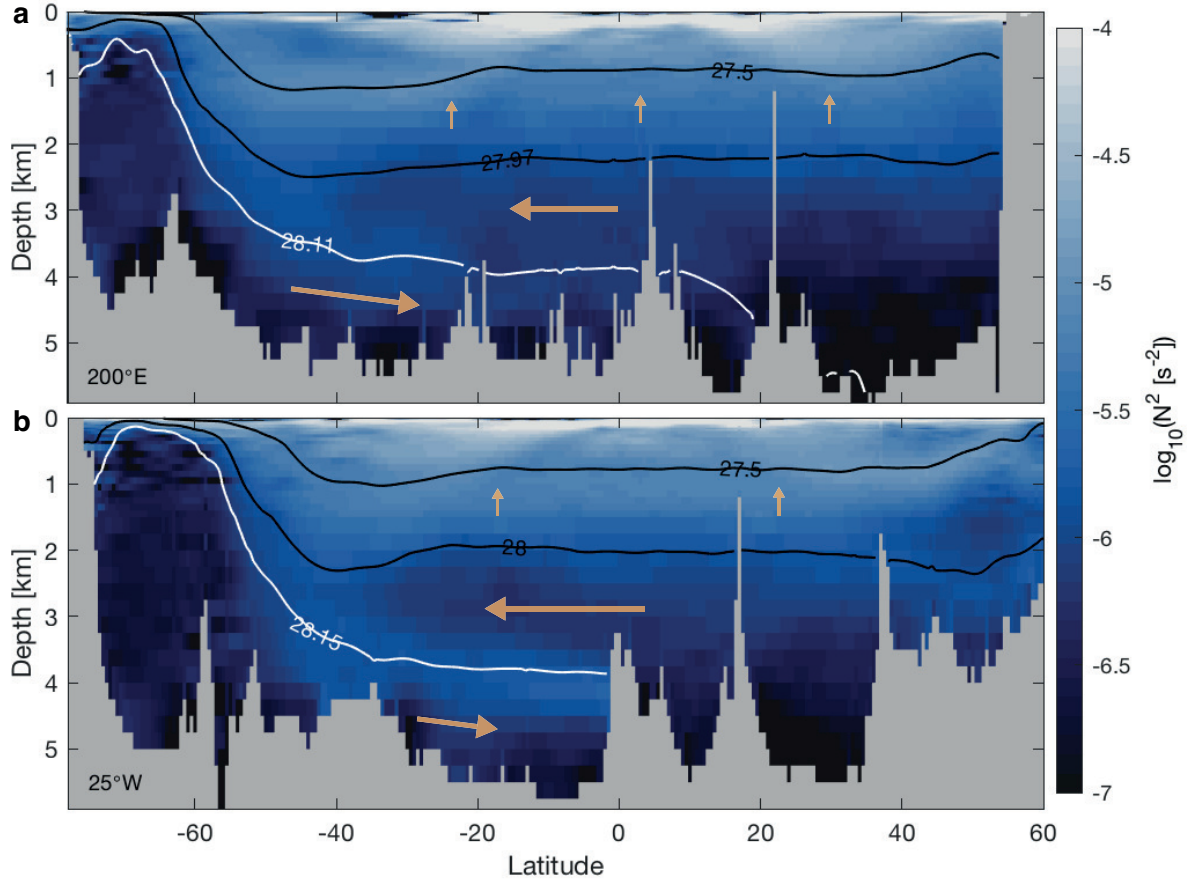


**Figure 7:** Squared buoyancy frequency ( $N^2 = -\frac{g}{\rho} \frac{\partial \rho}{\partial z}$ ) along 200°E/160°W **(a)** and 25°W **(b)** transects cutting through the Pacific and Atlantic basins, respectively. Data from Gouretski and Koltermann (2004). Orange arrows illustrate the circulation implied by diapycnal transports diagnosed in Figure 8. In the Atlantic, the southward mid-depth flow is stronger than the bottom northward flow due to North Atlantic Deep Water inflow (Talley 2013, Lozier et al. 2019). White contours are the neutral density surfaces of meridional flow reversal, coinciding with a local stratification maximum. Black contours are density surfaces enclosing the Munk regime characterized by weak mixing-driven upwelling (see section 6a and Fig. 8). This regime’s density range overlies that of abundant seafloor (de Lavergne et al. 2017; Fig. 12) and underlies that of intermediate waters (Naveira Garabato et al. 2014).

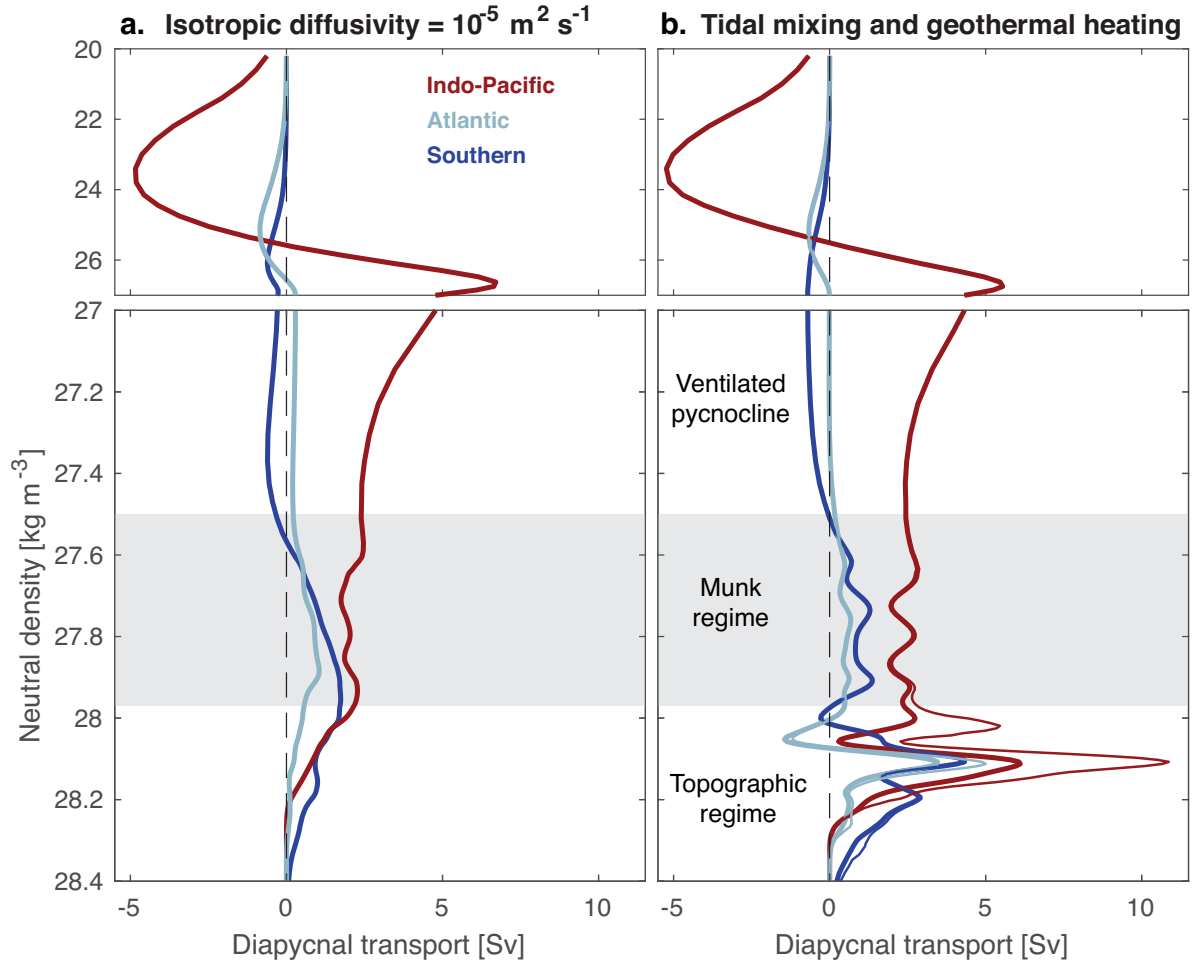


**Figure 8:** Estimated diapycnal upwelling due to isotropic mixing, split into Indo-Pacific (red), Atlantic (light blue) and Southern (dark blue) oceans. The Southern Ocean is defined as south of 32°S. **a**, Constant isotropic diffusivity of 10<sup>-5</sup> m<sup>2</sup> s<sup>-1</sup>. **b**, Realistic tidal mixing (thick curves), with added contribution of geothermal heating (thin curves). Positive values correspond to transport toward smaller densities (diapycnal upwelling). Where the shown transports increase upward, mixing causes volume loss or consumption; where transports decrease upward, mixing causes volume gain or formation. Regimes are defined in section 6 (see also Figs. 7 and 12). The employed climatological hydrography is that of Gouretski and Koltermann (2004). Tidal mixing rates are from de Lavergne et al. (2020) and geothermal heat fluxes from Lucazeau (2019). The methodology follows that of de Lavergne et al. (2016).

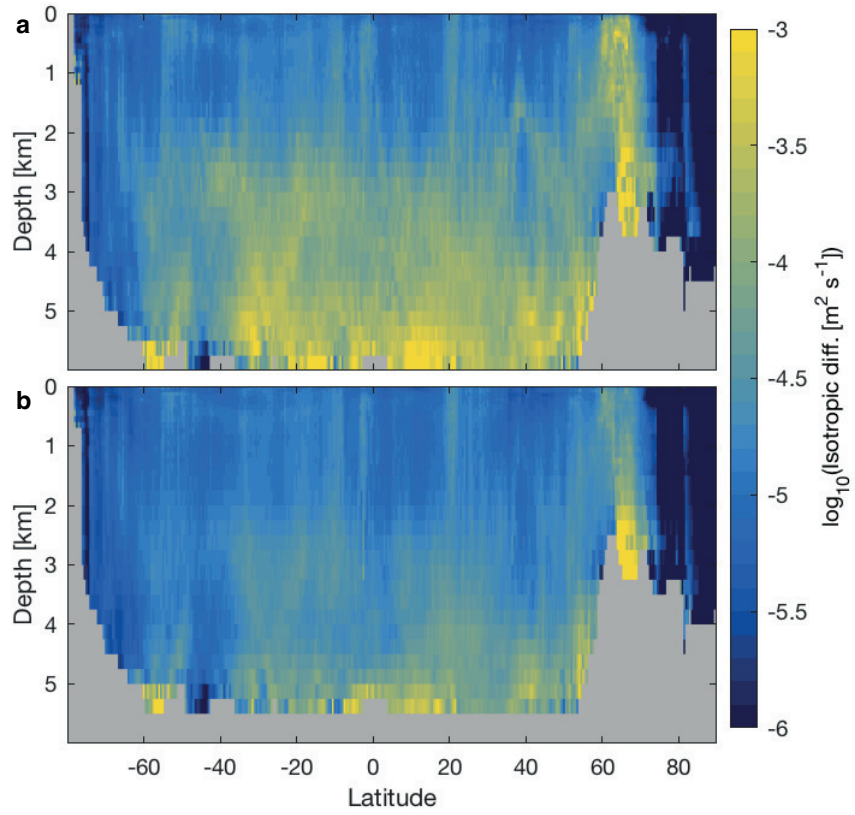


**Figure 9:** Zonal means of the isotropic diffusivity induced by internal tides, as mapped by de Lavergne et al. (2020). **a**, Global zonal mean diffusivity, where the average is weighted by  $|\frac{\partial \rho}{\partial z}|$  so that mean values relate to density fluxes. **b**, Same as **a**, with the bottom 500 m of every water column excluded from the averaging.

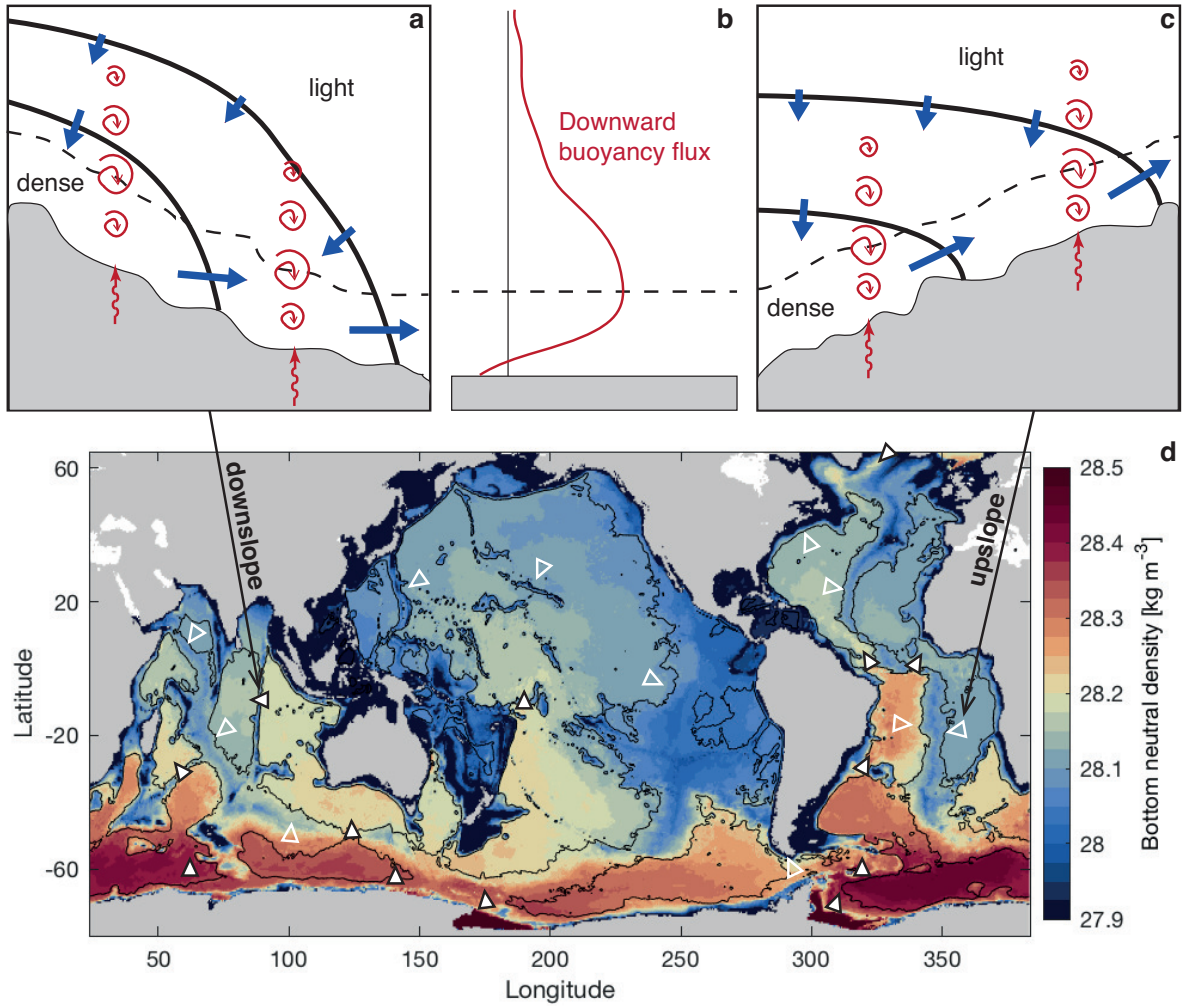


**Figure 10:** **a-c**, Downslope (**a**) and upslope (**c**) currents tied to near-bottom diffusive buoyancy fluxes (**b**). Boundary-catalyzed turbulence (red spirals) and geothermal heat fluxes (red wiggly arrows) drive a convergent buoyancy flux within a thin bottom layer (dashed line) and a divergent buoyancy flux above it. The bottom buoyancy gain is balanced by along-slope flow, whereas the buoyancy loss above is balanced by sinking of interior waters (blue arrows). Thick black lines represent density surfaces. **d**, For illustration, some representative locations of intense cross-density flows (triangles; filled for downslope, empty for upslope) are shown on top of shaded bottom neutral density (Gouretski and Koltermann 2004). The 4 km bathymetric contour is shown in black. Strong downslope flows filling the abyss are found downstream of major dense water formation sites and sills, while upslope cross-density transport is thought to be concentrated along the rough flanks of ridges.

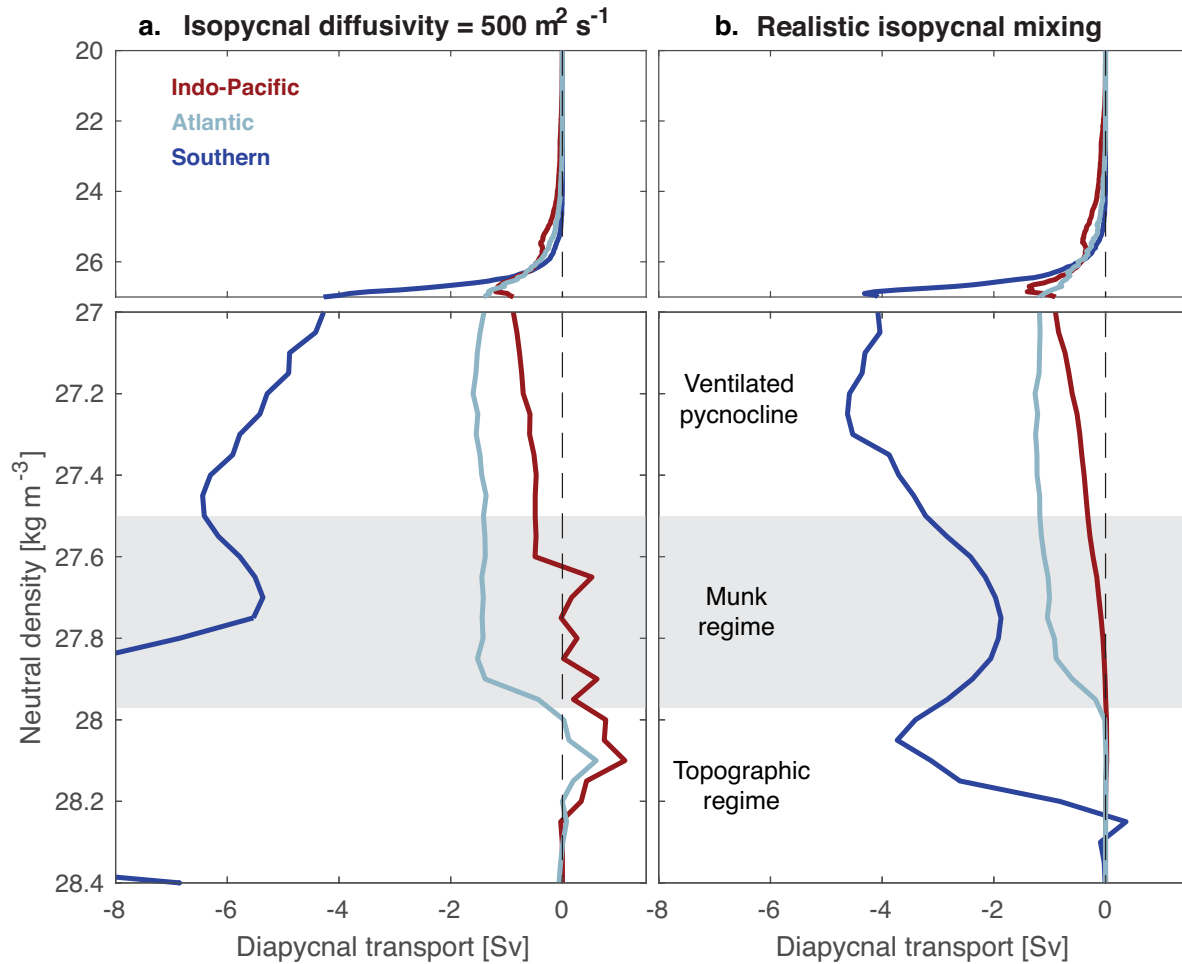


**Figure 11:** Estimated diapycnal upwelling due to isopycnal mixing, split into Indo-Pacific (red), Atlantic (light blue) and Southern (dark blue) oceans. The Southern Ocean is defined as south of 32°S. **a.** Constant isopycnal diffusivity of  $500 \text{ m}^2 \text{ s}^{-1}$ . **b.** Varying isopycnal diffusivity mapped by Groeskamp et al. (2020). The calculation follows the methodology of Groeskamp et al. (2016) and is based on monthly climatological hydrographic fields from World Ocean Atlas 2018 (Locarnini et al. 2018, Zweng et al. 2018). Downwelling outside the axis range in panel **a**, at densities greater than  $27.8 \text{ kg m}^{-3}$ , occurs near the Antarctic continent and could be an artefact of poor observational coverage; more realistic diffusivities used in **b** eliminate these large transports.

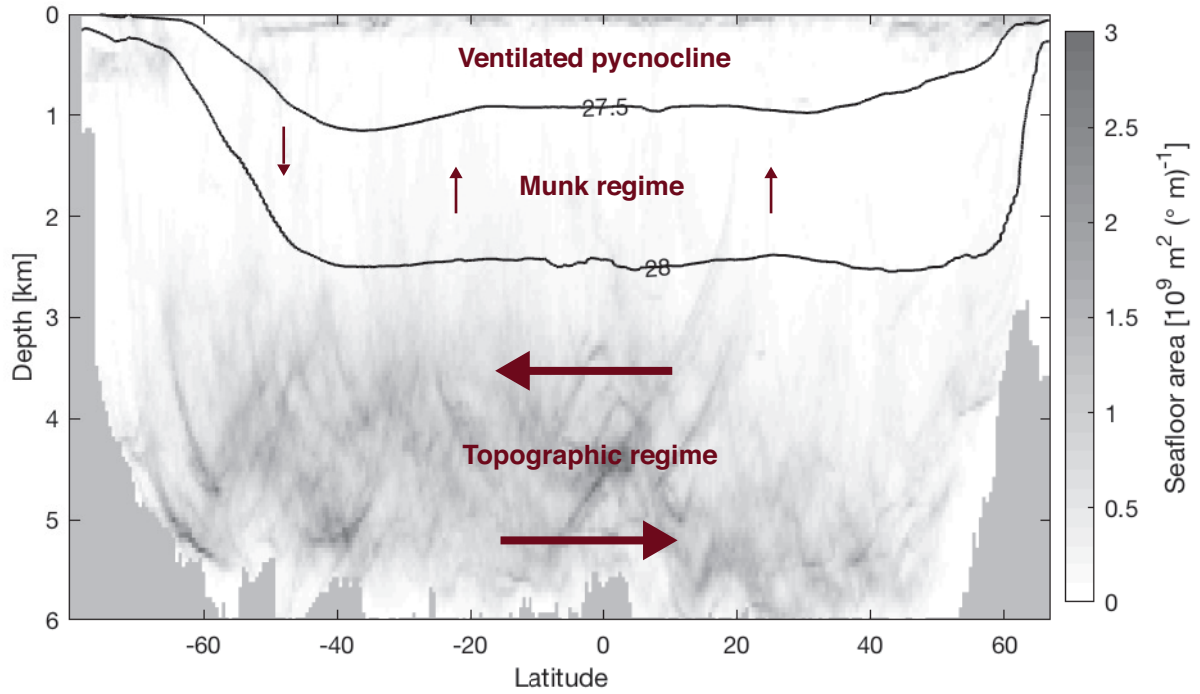


**Figure 12:** Proposed circulation regimes. The zonally summed seafloor area (in square meters per unit depth and per latitude degree) is shaded. Black curves represent the pseudo-depth of 27.5 and 28  $\text{kg m}^{-3}$  neutral density surfaces, where the pseudo-depth of density surfaces is found by filling each latitude band from the bottom up with ocean grid cells ordered from dense to light. The Munk regime, between the two black contours, hosts moderate mixing-driven vertical circulation. The underlying topographic regime is characterized by northward abyssal flow and southward deep flow, both strongly influenced by topography and near-bottom mixing. The ventilated pycnocline hosts swift upper-ocean flows influenced by mixing near the surface.



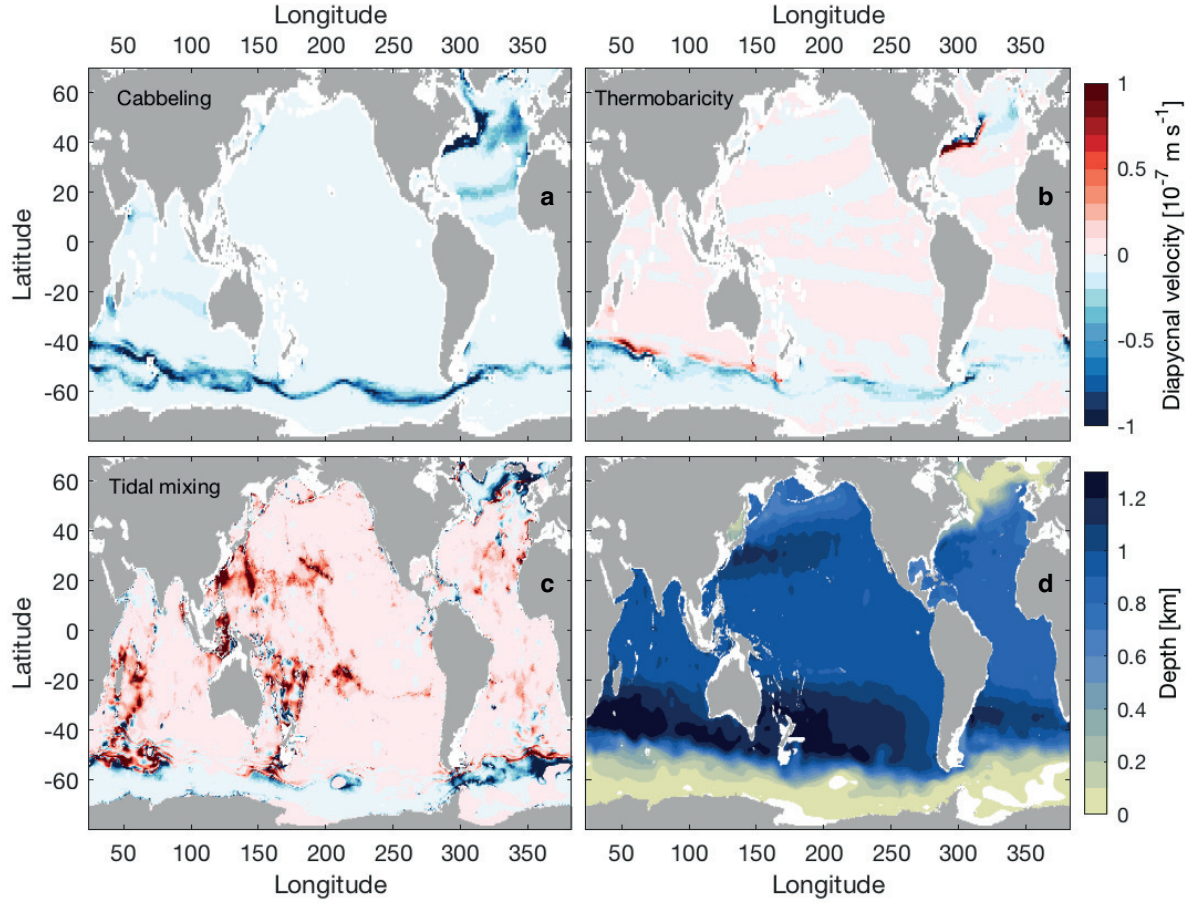


**Figure 13:** Estimated diapycnal velocities across the 27.5 kg m<sup>-3</sup> surface. **a,b**, Velocity implied by isopycnal mixing via cabbeling (**a**) and thermobaricity effects (**b**), calculated according to Groeskamp et al. (2016), using World Ocean Atlas 2018 monthly hydrography (Locarnini et al. 2018, Zweng et al. 2018) and isopycnal diffusivities from Groeskamp et al. (2020). **c**, Velocity implied by tidal mixing calculated according to de Lavergne et al. (2016) using isotropic diffusivities from de Lavergne et al. (2020). **d**, Depth of the 27.5 kg m<sup>-3</sup> neutral density surface in the climatology of Gouretski and Koltermann (2004). This density surface was chosen to separate the ventilated pycnocline from the Munk regime (Fig. 12).